

THESIS

DEVELOPMENT AND VERIFICATION OF A MINIATURE CONE
PENETRATION TEST

Submitted by

Kubra Kahramanoglu

Department of Civil & Environmental Engineering

In partial fulfillment of the requirements

For the Degree of Master of Science

Colorado State University

Fort Collins, Colorado

Spring 2019

Master's Committee:

Advisor: Christopher A. Bareither

Joseph Scalia
John Singleton

Copyright by Kubra Kahramanoglu 2019

All Rights Reserved

ABSTRACT

DEVELOPMENT AND VERIFICATION OF A MINIATURE CONE PENETRATION TEST

The objectives of this research were to design and validate a miniature cone penetration test (MCPT) system for testing fine-grained soils. The system included a commercially-available miniature piezocone and a 300-mm-diameter, rigid-wall, calibration chamber. Three different materials were used in this study: (i) Ottawa sand, (ii) fine synthetic tailings (FST), and (iii) coal combustion product (CCP). Ottawa sand was used to evaluate repeatability of the MCPT apparatus and verify results via comparison to literature. The FST was a mixture of kaolin clay and silica flour, whereas CCP was primarily sand and silt and collected from a coal ash impoundment in North America. These two materials were tested to assess undrained and drained shear behavior and compare with previously measured shear strength. Replicate MCPTs conducted on Ottawa sand at three different relative densities indicated that the MCPT was repeatable. The assessment of tip resistance and sleeve friction in the Ottawa sand MCPTs were used to identify a functional depth of penetration whereby the friction sleeve was fully mobilized. Values of tip resistance and sleeve friction obtained from the MCPT at these depths of penetration were taken as representative of the specimen and subsequently validated via comparison to literature. Pore water pressure developed during cone penetration in the Ottawa sand and CCP were similar and indicative of drained conditions, whereas large, positive pore pressures in the FST were indicative of undrained conditions. The undrained shear strength estimated from MCPTs on FST (13 and 35 kPa) compared favorably and had a good agreement with undrained shear strength from triaxial tests. The effective stress friction angle for CCP based on MCPT (28.7° and 30.4°) yielded a conservative estimate relative to a previously determined effective friction angle via triaxial testing (36°).

ACKNOWLEDGEMENTS

First and foremost, I would like to express my deepest gratitude to my supervisor, Dr. Christopher A. Bareither for his support, guidance, and suggestions in this thesis research. Without his patience and encouragement, this thesis would not have been completed. I also would like to extend my sincere appreciations to the committee members, Assist. Prof. Joseph Scalia IV and Assist. Prof. John Singleton for their constructive criticism and suggestions on the thesis.

I owe a particular gratitude to Logan Pokallus for his help in developing the laboratory setup and its software. I would also like to thank to my colleagues in GeoGroup for their moral supports and encouragements.

I am very grateful to my dear friends, Selma and Şerif Kaya, and Halil Sözeri for their endless emotional supports and love. I wish to thank my family for their continuous support and encouragement throughout the preparation of this thesis. Last but not least, I would like to express my special thanks to Onur Gölbaşı who has always been with me during this period and who always encouraged me to realize my full potential.

TABLE OF CONTENTS

ABSTRACT.....	ii
ACKNOWLEDGEMENTS	iii
LIST OF TABLES.....	vi
LIST OF FIGURES	vii
LIST OF SYMBOLS	x
CHAPTER 1: INTRODUCTION.....	1
1.1 Research Motivation.....	1
1.2 Objectives and Scope of Research.....	2
CHAPTER 2: BACKGROUND	3
2.1 Cone Penetration Test (CPT)	3
2.1.1 General Characteristics.....	4
2.1.2 Interpretation of CPT Data	5
2.1.2.1 Peak Friction Angle (ϕ')	5
2.1.2.2 Undrained Shear Strength	6
2.2 Calibration Chambers for CPT	7
CHAPTER 3: DEVELOPMENT OF A MINIATURE CONE PENETROMETER.....	13
3.1 Piezocone.....	13
3.2 Mini-Piezocone Penetration System	13
3.3 Calibration Chamber.....	14
3.4 Vertical Loading System	14
3.5 Data Acquisition and Control System.....	15
CHAPTER 4: MATERIALS AND METHOD	21
4.1 Materials.....	21
4.2 Miniature Cone Penetration Test (MCPT)	22
CHAPTER 5: RESULTS AND DISCUSSION	29
5.1 MCPT Measurements on Ottawa Sand	29
5.1.1 The Effect of Increase in Relative Density on q_c and f_s	31
5.1.2 Soil Behavior Type	32
5.1.3 Friction Angle	33
5.2 MCPT Measurements on FST and CCP	33
5.2.1 Penetration Behavior of FST	34
5.2.2 Penetration Behavior of CCP	35

5.2.3 MCPT Comparison.....	36
5.2.4 Undrained Shear Strength Assessment of FST.....	37
5.2.5 Effective Stress Friction Angle Assessment of CCP.....	38
5.3 Practical Implications.....	38
CHAPTER 6: SUMMARY, CONCLUSIONS, AND FUTURE WORK.....	60
6.1 Summary and Conclusions.....	60
6.2 Future Work.....	61
REFERENCES.....	62
APPENDIX A: DESIGN DRAWINGS.....	66
APPENDIX B: CONSOLIDATION DATA.....	69

LIST OF TABLES

Table 4.1	Geotechnical characteristics of the materials.....	25
Table 4.2	Penetration rates of the specimens based on the drainage conditions.	26
Table 5.1	Summary of miniature cone penetration tests conducted on Ottawa Sand.	40
Table 5.2	Comparison between internal effective stress friction angles of Ottawa Sand reported in literature and friction angles predicted based on miniature cone penetration tests in this study.	41
Table 5.3	Summary of miniature cone penetration tests conducted on fine synthetic tailings (FST) and coal combustion product (CCP), and estimated shear strength for each material.....	42

LIST OF FIGURES

Fig. 2.1.	Schematic of a cone penetration test (CPT) and common piezocone used in accordance with the ASTM D 5778 procedures (Mayne 2007).....	9
Fig. 2.2.	Relationships between the effective friction angle (ϕ') and the normalized cone resistance for (a) sands (Mayne 2014) (b) silts and clays (Mayne 2005).	10
Fig. 2.3.	Schematic of a calibration chamber setup for a cone penetration test (Lee et al. 2008).....	11
Fig. 2.4.	Boundary condition types in calibration chamber tests (Salgado et al. 1998).....	12
Fig. 3.1.	Schematic of the miniature cone penetration test system (not to scale).....	16
Fig. 3.2.	Photograph of the miniature cone penetration test system.	17
Fig. 3.3.	Schematic of the miniature piezocone.	18
Fig. 3.4.	Photograph of the mini-piezocone and DAQ system of CPT.	19
Fig. 3.5.	Relationships of vertical displacement rate of the mini-piezocone versus air pressure applied to the hydraulic reservoir for two sets of experiments (a and b). The Opening refers to the position on the flow control valve, where 5 corresponds to the largest opening.	20
Fig. 4.1.	Particle-size distributions for Ottawa sand, fine synthetic tailings (FST), and coal combustion product (CCP).	27
Fig. 4.2.	Schematic of the calibration chamber and specimen boundaries for the fine synthetic tailings and coal combustion product.....	28
Fig. 5.1.	Relationships of (a) tip resistance (q_c), (b) sleeve friction (f_s), and (c) friction ratio (R_f) as a function of penetration depth for miniature cone penetration tests on Ottawa sand at final relative densities ($Dr_f \approx 24\%$).....	43
Fig. 5.2.	Relationships of (a) tip resistance (q_c), (b) sleeve friction (f_s), and (c) friction ratio (R_f) as a function of penetration depth for miniature cone penetration tests on Ottawa sand at final relative densities ($Dr_f \approx 29\%$).....	44
Fig. 5.3.	Relationships of (a) tip resistance (q_c), (b) sleeve friction (f_s), and (c) friction ratio (R_f) as a function of penetration depth for miniature cone penetration tests on Ottawa sand at final relative densities ($Dr_f \approx 43\%$).....	45
Fig. 5.4.	Relationships of (a) tip resistance (q_c), (b) sleeve friction (f_s), and (c) friction ratio (R_f) as a function of normalized specimen depth for all six miniature cone penetration tests on Ottawa sand. Normalized specimen depth = penetration depth below specimen surface / specimen thickness. Final relative densities (Dr_f) listed in the legend.....	46

Fig. 5.5. Relationships of (a) tip resistance and (b) sleeve friction versus consolidated relative density of the Ottawa sand specimens.....	47
Fig. 5.6. Comparison of cone tip resistance versus consolidated relative density relationships from miniature cone penetration tests on Ottawa sand conducted in this study and in Damavandi-Monfared and Sadrekarimi (2015). All tests were conducted for sand consolidated under a vertical effective stress (σ'_v) of 100 kPa.....	48
Fig. 5.7. Comparison of q_{tt} values from MCPT experiments of this study with other experiments conducted by Mayne (2006).....	49
Fig. 5.8. Relationship of normalized tip resistance versus normalized friction ratio from Robertson (1990) that includes soil identification zones based on cone penetration test results. Data from the miniature cone penetration tests conducted in this study on Ottawa sand are plotted as black squares.	50
Fig. 5.9. Compilation of triaxial data and empirical relationships on clean Ottawa sands between the effective friction angle (ϕ') and normalized cone resistance from a cone penetration test. Normalized cone resistances from miniature cone penetration tests in this study were used to estimate ϕ' based on the relationship in Kulhawy and Mayne (1990).	51
Fig. 5.10. Relationships of (a) tip resistance (q_c), (b) sleeve friction (f_s), and (c) pore water pressure as a function of penetration depth for the miniature cone penetration test on FST consolidated under a vertical effective stress (σ'_v) of 50 kPa.....	52
Fig. 5.11. Relationships of (a) tip resistance (q_c), (b) sleeve friction (f_s), and (c) pore water pressure as a function of penetration depth for the miniature cone penetration test on FST consolidated under a vertical effective stress (σ'_v) of 100 kPa.....	53
Fig. 5.12. Relationships of (a) tip resistance (q_c), (b) sleeve friction (f_s), and (c) pore water pressure as a function of penetration depth for the miniature cone penetration test on CCP consolidated under a vertical effective stress (σ'_v) of 40 kPa.	54
Fig. 5.13. Relationships of (a) tip resistance (q_c), (b) sleeve friction (f_s), and (c) pore water pressure as a function of penetration depth for the miniature cone penetration test on CCP consolidated under a vertical effective stress (σ'_v) of 88 kPa.	56
Fig. 5.14. Relationships of (a) tip resistance (q_c), (b) sleeve friction (f_s), and (c) friction ratio (R_f) as a function of normalized specimen depth for all miniature cone penetration tests on FST and CCP. Normalized specimen depth = penetration depth below specimen surface / specimen thickness. Grey area indicates the range of normalized depths at which 100% sleeve frictional resistance was mobilized.....	57
Fig. 5.15. Relationships of pore water as a function of normalized specimen depth for miniature cone penetration tests on (a) Ottawa sand, (b) Ottawa sand with a modified pore pressure scale, and (c) FST and CCP. Normalized specimen depth = penetration depth below specimen surface / specimen thickness. The	

modified pore pressure scale for (b) is the same scale as used in (c) to show a more direct comparison between pore pressure measured in the three different materials.	58
Fig. 5.16. Relationships between undrained shear strength and mean effective stress at the end of consolidation for FST based on miniature cone penetration tests in this study and consolidated undrained triaxial compression tests in Hamade (2017).	59
Fig. A.1. Dimensions of the specimen cell.....	66
Fig. A.2. Drawing views of the cross bar from different perspectives.....	67
Fig. A.3. Drawing views of the bottom plates from different perspectives	68
Fig. B.1. Temporal trends of (a) excess pore water pressure and (c) vertical deformation of the specimen surface for the FST in the miniature cone penetration test tested under a vertical effective stress (σ'_v) of 50 kPa.	69
Fig. B.2. Temporal trends of (a) excess pore water pressure and (c) vertical deformation of the specimen surface for the FST in the miniature cone penetration test tested under a vertical effective stress (σ'_v) of 100 kPa.	70
Fig. B.3. Comparison of void ratio versus vertical effective stress data for FST from the two miniature cone penetration tests and oedometer data from Gorakhki and Bareither (2018) and Tian (2017).	71
Fig. B.4. Temporal trends of (a) excess pore water pressure and (c) vertical deformation of the specimen surface for the CCP in the miniature cone penetration test tested under a vertical effective stress (σ'_v) of 40 kPa.	72
Fig. B.5. Temporal trends of (a) excess pore water pressure and (c) vertical deformation of the specimen surface for the CCP in the miniature cone penetration test tested under a vertical effective stress (σ'_v) of 88 kPa.	73
Fig. B.6. Comparison of void ratio versus vertical effective stress data for CCP from miniature cone penetration tests and seepage-induced consolidation (SICT), direct shear (DS), triaxial, and vane shear tests conducted by Herweynen (2018).	74

LIST OF SYMBOLS

a	net cone area ratio	N_{kt}	cone factor
a'	value of attraction	N_m	cone resistance number
A_c	tip surface area	p'	mean effective stress
A_s	surface area of the friction sleeve	PI	plasticity index
BC1	boundary condition (constant radial and vertical stress)	PSD	particle size distribution
BC2	boundary condition (constant volume)	q_c	cone tip resistance
BC3	boundary condition (constant vertical stress and zero radial displacement)	Q_c	thrust force on cone tip
BC4	boundary condition (constant radial stress and zero vertical displacement)	Q_f	summation of thrust forces on the cone tip and friction sleeve
B_q	pore parameter ratio	q_t	corrected cone tip resistance
c'	effective cohesion	q_{t1}	normalized cone resistance
CCP	coal combustion product	R_f	friction ratio
CPT	cone penetration test	S_u	undrained shear strength
c_v	coefficient of consolidation	u	pore water pressure
DAQ	data acquisition	u_0	static pore water pressure
D_c	calibration chamber diameter	u_2	pore water stresses behind the tip
d_c	diameter of the penetrometer	USCS	unified soil classification system
d_{50}	mean particle diameter	V	a normalized penetration rate
d_{max}	maximum particle size	v	penetration rate

Dr_f	relative density after consolidation	MCPT	miniature cone penetration test
Dr_i	initial relative density	V_d	normalized penetration rate for drained conditions
e_i	initial void ratio	V_d	penetration rate for drained condition
e_{max}	maximum void ratio	V_{un}	normalized penetration rate for undrained conditions
e_{min}	minimum void ratio	V_{un}	penetration rate for undrained condition
f_s	sleeve friction resistance	w_{opt}	optimum water content
F_s	thrust force on friction sleeve	ϕ'	effective friction angle
FST	fine synthetic tailings	σ'_{v0}	effective overburden stress
G_s	specific gravity of solids	σ_{v0}	total overburden stress
k	hydraulic conductivity	σ_v'	vertical effective stress
K_o	at rest earth pressure	σ_{atm}	a reference stress equal to one atmosphere
LL	liquid limit	γ_{dmax}	maximum dry unit weight
ML	low plasticity silt		

CHAPTER 1: INTRODUCTION

1.1 Research Motivation

Determining the engineering properties of in situ soils can be achieved via collection and subsequent testing of undisturbed samples or in situ testing. Although both methods are used commonly in geotechnical engineering practice, the available technology and competitive cost of in situ testing has created a broad spectrum of tests to address the needs of geotechnical engineers. Common in situ tests include the standard penetration test, cone penetration test, vane shear test, flat plate dilatometer test, and pressuremeter test (Mayne 2007). Each of these tests have advantages and disadvantages, and all are capable of yielding indirect measurements of soil behavior that can be used to determine relevant soil properties for engineering design.

The cone penetration test (CPT) is rapidly becoming a preferred in situ test for geotechnical engineers due to continuous measurement with penetration, established theoretical basis for data interpretation, and generation of repeatable and reliable data (Robertson and Cabal 2015). A typical CPT involves pushing a cone-shaped probe (piezocone) into the soil at a constant rate of penetration (e.g., 20 mm/s), and yields continuous measurements of tip resistance, sleeve friction, and pore water pressure. More advanced piezocones can incorporate a broad range of sensors for geophysical and pore water chemistry measurements. Tip resistance measured by the piezocone provides a measure of the shear resistance to an induced load, while sleeve friction provides a measure of frictional resistance. These measurements can be connected empirically to soil composition and soil engineering properties (e.g., Mayne 2014; Uzielli et al. 2013; Gorman et al. 1975; Kulhawy and Mayne 1990; Robertson 1990; Senneset et al. 1989).

The development of piezocones for CPT and empirical relationships for linking piezocone measurements to soil engineering properties has relied on the use of laboratory-scale calibration chambers. Calibration chambers provide control on stress conditions and soil characteristics such that the state of a soil is known during a penetration test. The two types of calibration chambers

used for CPT are rigid-wall chambers, which include a boundary condition of zero lateral strain, and flexible-wall chambers, which allow lateral strain but control lateral stress (Holden 1971; Ghionna and Jamiolkowski 1991; Salgado et al. 1998). Laboratory calibration chambers for CPT continue to have an important role in developing and accessing new piezocones and developing new empirical correlations to geotechnical engineering properties. The majority of laboratory calibration chamber tests have been conducted on sandy soils since preparation and testing is quicker and easier relative to fine-grained soils (e.g. Kumar and Raju 2009; Salgado et al. 1998; Been et al. 1986). Furthermore, calibration chambers for medium to dense sands require a relatively large aspect ratio between chamber diameter and piezocone diameter to minimize the influence of chamber boundaries. Thus, the assessment of smaller-scale calibration chambers has not been thoroughly evaluated with the notion of developing an economically-sized calibration chamber for evaluating fine-grained soils.

1.2 Objectives and Scope of Research

The objective of this study was to design and verify a laboratory-scale miniature cone penetration test (MCPT) that incorporated a calibration chamber designed for testing fine-grained soils. A commercially-available mini-piezocone was used in the MCPT system. Following verification of the MCPT system using Ottawa sand, penetration tests were conducted on two slurry-prepared materials: fine synthetic tailings (FST) and coal combustion product (CCP). The FST was a laboratory-prepared mixture of kaolin clay and silica powder that represented the particle-size distribution of a common fine-grained mine tailings. The CCP was collected from a coal ash impoundment in North America. Results from the MCPTs on CCP and FST were compared to previously measured shear strength parameters for each of the materials to validate that the MCPT can be used to assess fine-grained materials prepared from slurries.

CHAPTER 2: BACKGROUND

2.1 Cone Penetration Test (CPT)

The cone penetration test has become a practical in situ test for soil analysis due to quick and economic implementation since the first cone penetrometer was developed in 1932 in the Netherlands (Lunne et al. 1997). The CPT provides a continuous soil profile without the need for boring or sampling. Moreover, CPT provides multiple independent readings during penetration compared to traditional rotary drilling and borehole sampling (Mayne 2010).

The CPT is used for evaluating geotechnical characteristics and engineering properties of soil as a function of depth. In a common CPT, tip resistance (q_c), sleeve friction (f_s), and pore water pressure (u) are measured (ASTM D3441, 2016). Soil characterization and engineering parameters, such as relative density, friction angle, over-consolidation ratio, pile bearing capacity, and liquefaction potential, can be determined from CPT results (Mayne 2010; Damavandi-Monfared 2014).

A schematic of a CPT setup and piezocone used in a common ASTM test procedure is shown in Fig. 2.1. Key features of a CPT are a reaction force used to push the piezocone into the ground (e.g., truck weight in Fig. 2.1), a piezocone, and rod extensions to attach to the piezocone as depth of penetration increases. There are many different scales of CPT systems, which vary from small, mobile units with miniature piezocones (mini-piezocone) to large trucks that provide the necessary reaction force for deep penetration (e.g., > 100 m). The standard piezocone according to ASTM D3441 (2016) is a mechanical cone with a diameter of 35.7 mm, angle of 60° from cone shaft to the tip, and 10-cm² surface area of the cone tip. Mini-piezocones have been manufactured with cross-sectional areas ranging from 1 cm² to 5 cm².

2.1.1 General Characteristics

Test procedures for mechanical CPT systems are outlined in ASTM D3441, whereas test procedures for electronic cone systems are outlined in ASTM D5778. The mechanical CPT is the baseline test that yields tip resistance of the conical point and frictional resistance of the cylindrical sleeve (ASTM D3441, 2016). Pore water pressure is also commonly measured.

Piezocone measurements recorded during a CPT are input in equations outlined in ASTM-D3441 to yield cone tip resistance (q_c) and sleeve friction resistance (f_s) in units of MPa:

$$q_c = 1000 \frac{Q_c}{A_c} \quad (2.1)$$

$$f_s = 1000 \frac{F_s}{A_s} \quad (2.2)$$

$$F_s = Q_f - Q_c \quad (2.3)$$

where Q_c is thrust force on the cone tip (kN), A_c is surface area of the cone tip, F_s is thrust force on the friction sleeve (kN), and A_s is surface area of the friction sleeve. Moreover, Q_f is the summation of thrust forces on the cone tip and friction sleeve. A common parameter computed from q_c and f_s is the friction ratio (R_f) in percent, which is in Eq. 2.4.

$$R_f = 100 \frac{f_s}{q_c} \quad (2.4)$$

Cone penetration is commonly conducted at a penetration rate of 20 mm/s. This penetration rate has the propensity to develop undrained conditions in fine-grained soils that include clay minerals. However, partially-drained or fully-drained conditions can develop in sands and silt-dominated fine-grained soils (Kim et al. 2008). Drainage conditions during CPT can be identified by accounting for probe size, penetration rate, and soil consolidation characteristics. To evaluate the effect of drainage conditions on CPT measurements, penetration rates can be converted to a dimensionless penetration rate.

Randolph and Hope (2004) developed a normalized penetration rate (V) as

$$V = \frac{v \cdot d_c}{c_v} \quad (2.5)$$

where v is penetration rate used in the CPT, d_c is diameter of the piezocone, and c_v is coefficient of consolidation of the soil evaluated. Normalized penetration rates have been back-calculated to determine target penetration rates for drained or undrained conditions, and Kim et al. (2008) report that complete undrained conditions develop for $V \geq 10$ and complete drained conditions develop for $V \leq 4$. Cone penetration test conditions (e.g., v , d_c , and/or c_v) that yield V between 4 and 10 are assumed to represent partially-drained conditions.

The excess pore pressure developed during penetration of a piezocone influences CPT results since q_c and f_s respond to the variations in pore pressure. Senneset and Janbu (1985) estimated a pore parameter ratio (B_q) during CPT as

$$B_q = \frac{(u_2 - u_0)}{(q_t - \sigma_{v0})} \quad (2.6)$$

where u_2 is pore water pressure measured by the piezocone during penetration, u_0 is static pore water pressure, q_t is corrected cone tip resistance, and σ_{v0} is total overburden stress. The q_t is computed as shown in Eq. 2.7 and relevant for silty and clayey soils.

$$q_t = q_c + (1 - a) \cdot u_2 \quad (2.7)$$

In sandy soils, q_c and q_t are equal since excess pore water pressure generated during piezocone penetration dissipates rapidly and measured pore water pressure on the piezocone is equivalent to hydrostatic pore water pressure (Mayne 2007).

2.1.2 Interpretation of CPT Data

2.1.2.1 Peak Friction Angle (ϕ')

Empirical correlations have been developed to estimate peak friction angle (ϕ') for a variety of soils. Kulhawy and Mayne (1990) conducted 24 calibration chamber CPTs on clean quartz

sandy soils, where cone resistance was adjusted for calibration chamber size effect (i.e., ratio of calibration chamber diameter to cone diameter) to yield the following relationship:

$$\phi' = 17.6^\circ + 11.0^\circ \cdot \log(q_{t1}) \quad (2.8)$$

where q_{t1} is normalized tip resistance. The normalized tip resistant is expressed as

$$q_{t1} = \left(\frac{q_t}{\sigma_{atm}} \right) / \left(\frac{\sigma'_{v0}}{\sigma_{atm}} \right)^{0.5} \quad (2.9)$$

where σ'_{v0} is effective overburden stress and σ_{atm} is a reference stress equal to one atmosphere (1 atm = 100 kPa). A graphical representation of the ϕ' versus q_{t1} relationships based on the calibration chamber data and triaxial tests is shown in Fig. 2.2a.

An effective stress-limit plasticity solution can be used to calculate ϕ' for clays and silts. Based on this solution, the cone resistance number (N_m) is defined as

$$N_m = (q_t - \sigma_{v0}) / \left(\frac{\sigma'_{v0}}{a'} \right) \quad (2.10)$$

where a' is attraction ($a' = c' \cot \phi'$) and c' is effective cohesion (Mayne 2005). Mayne (2005) formulated the calculation of ϕ' as a function of B_q and N_m as shown in Eq. 2.11.

$$\phi' = 29.5 \cdot B_q^{0.121} (0.256 + 0.336 \cdot B_q + \log N_m) \quad (2.11)$$

This derived solution is for normalized pore pressure values which vary between 0.1 and 1.0, and ϕ' changes between 20° and 45° (Fig. 2.2b).

2.1.2.2 Undrained Shear Strength

Undrained shear strength (S_u) depends on the mode of failure, strain rate, stress history, and soil anisotropy (Lunne et al. 1997). An estimation technique for peak S_u via q_t is

$$S_u = \frac{q_t - \sigma_{v0}}{N_{kt}} \quad (2.12)$$

where N_{kt} is cone factor that varies between 10 and 20 with an average of 15 (Lunne et al. 1997). According to Senneset et al. (1989), N_{kt} varies from 10 to 15 for normally consolidated clay and 15 to 19 for overconsolidated clay.

2.2 Calibration Chambers for CPT

A schematic of a general calibration chamber setup is shown in Fig. 2.3. Calibration chambers for CPT are specialty-designed cells in which a cone is pushed into a specimen of known density and stress. Experiments performed using a calibration chamber provide consistent results for interpretation of CPT measurements. Therefore, numeric values gathered at the end of calibration chamber experiments are considered reliable when deriving empirical relationships between soil properties and cone tip or sleeve friction resistance.

Compared to field testing, calibration chamber testing offer numerous advantages. In particular, calibration chambers offer control on the stress, density, and water content of a test specimen as well as the penetration rate and boundary conditions of the experiment. Uncertainties of soil inhomogeneity, in situ stress, and magnitude of stress can be removed via calibration chamber testing.

Scale effects in calibration chamber testing with piezocones develop due to variations in cell diameter and piezocone diameter (quantified as the ratio between the chamber diameter to piezocone diameter, D_c/d_c), which can influence test results (e.g., q_c). A penetration resistance theory was proposed to quantify chamber size effects by using relative density, stress state, intrinsic soil parameters, shear modulus, critical state friction angle, and void ratio. Relative density, stress state, and intrinsic soil parameters were identified as important variables for quantifying the magnitude of the chamber size effect on q_c , whereas critical state friction angle and void ratio were detected to be less influential on chamber size effect (Salgado et al. 1998).

Calibration chambers should be of sufficient size such that CPT results are not affected by the chamber boundaries. However, boundary conditions for calibration chambers have also

been shown to influence piezocone data. Salgado et al. (1998) summarized the boundary condition types in calibration chamber tests shown in Fig. 2.4: (i) constant radial and vertical stress (BC1); (ii) constant volume (BC2); (iii) constant vertical stress and zero radial displacement (BC3); and (iv) constant radial stress and zero vertical displacement (BC4). These boundary conditions include different lateral and bottom boundaries, whereby flexible-wall chambers provided constant lateral stress and rigid-wall chambers provide zero lateral displacement.

Ghionna and Jamiolkowski (1991) investigated boundary condition effects via changing the boundaries from constant stress to zero deformation (i.e., rigid boundaries). The measured q_c during CPT in a calibration chamber was influenced by the boundary conditions. Under constant boundary stress, larger piezocones yielded lower q_c . In addition, stress distribution in the specimen was not uniform when the calibration chamber had rigid bottom and top boundaries.

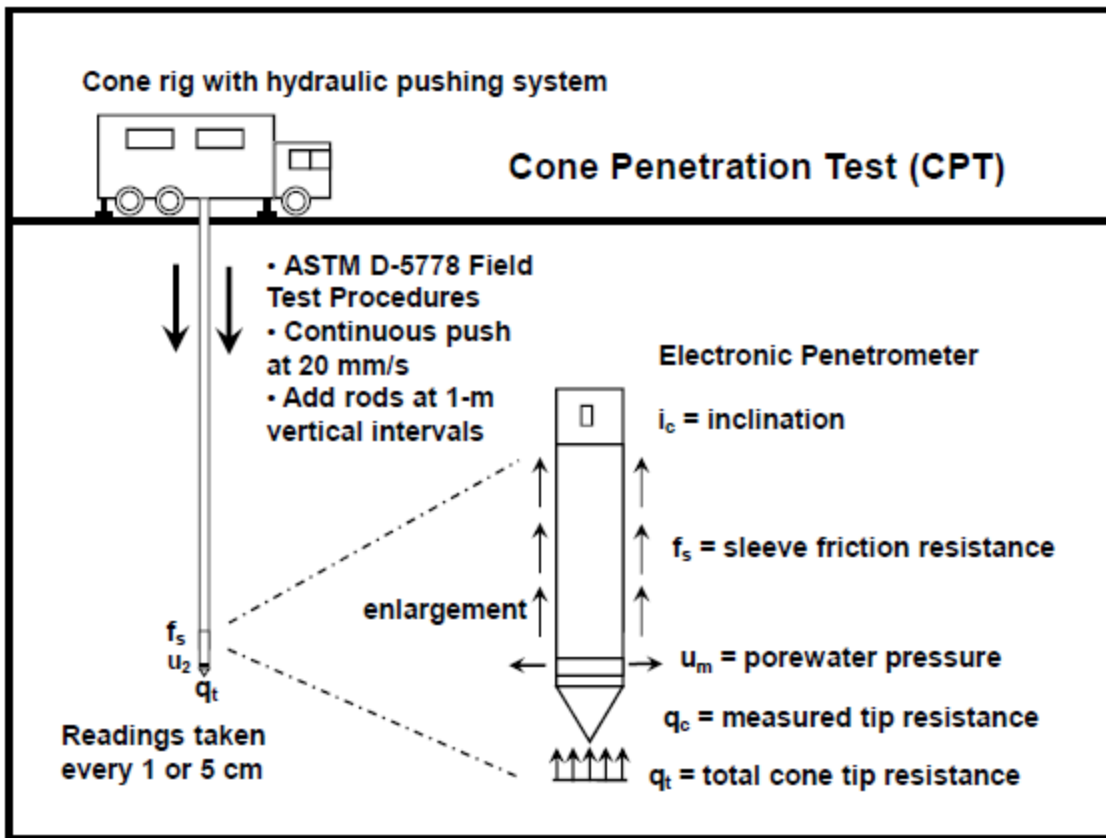
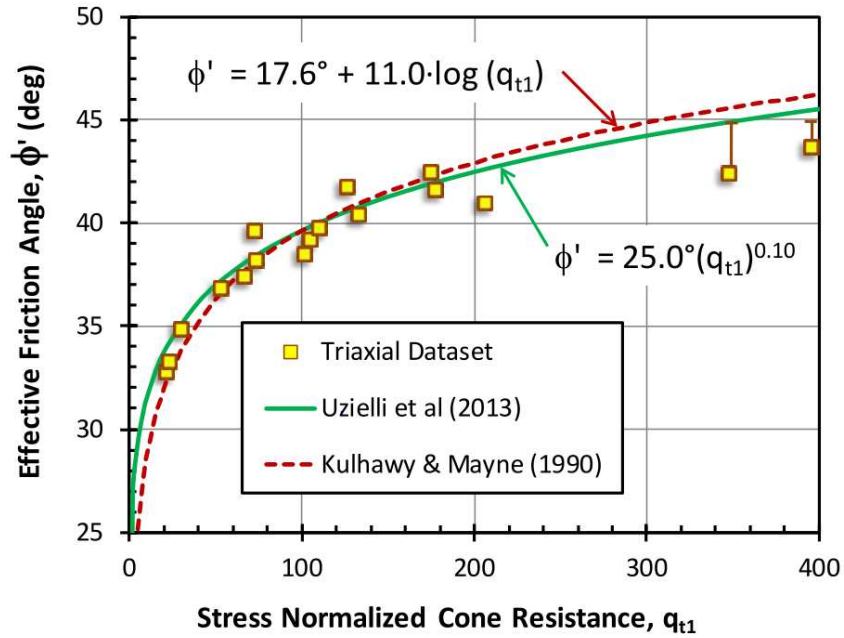
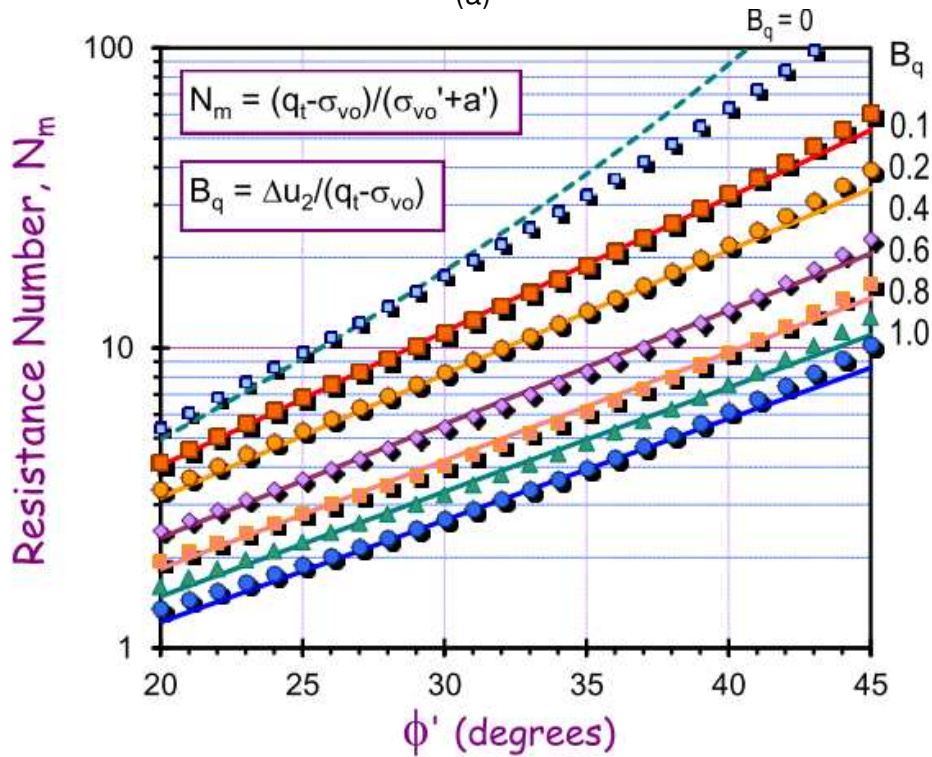


Fig. 2.1. Schematic of a cone penetration test (CPT) and common piezocone used in accordance with the ASTM D 5778 procedures (Mayne 2007).



(a)



(b)

Fig. 2.2. Relationships between the effective friction angle (ϕ') and the normalized cone resistance for (a) sands (Mayne 2014) (b) silts and clays (Mayne 2005).

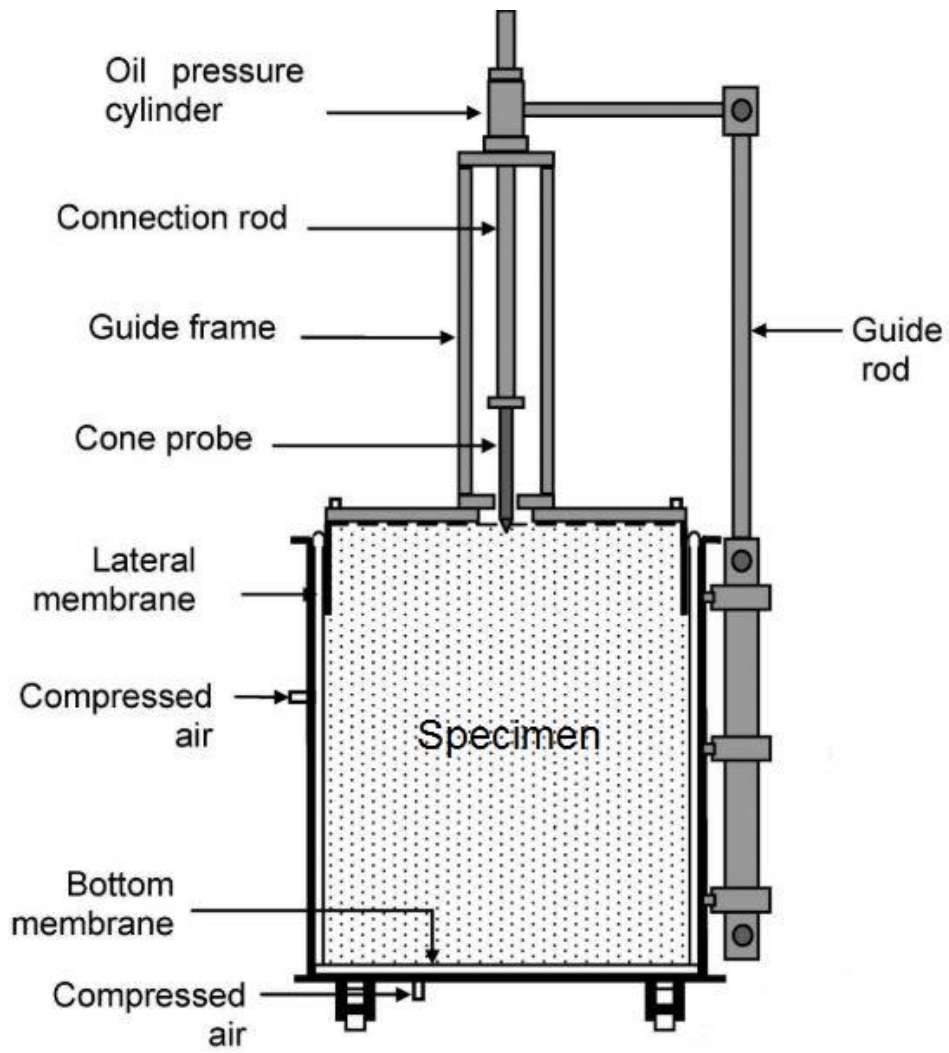
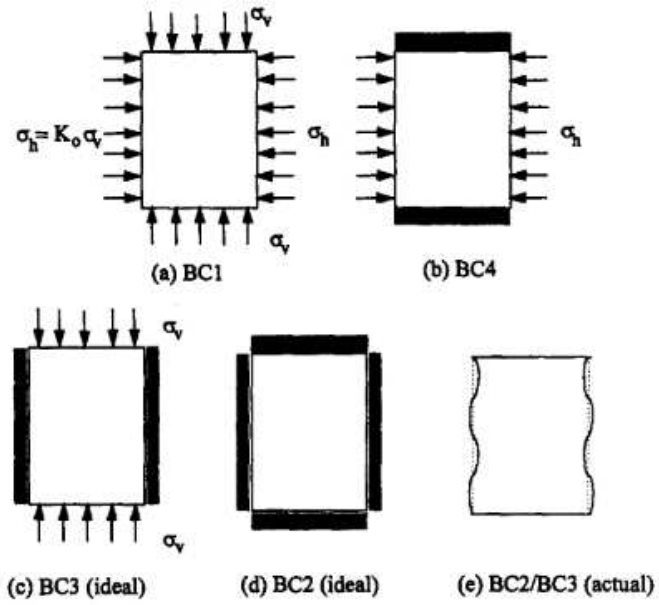


Fig. 2.3. Schematic of a calibration chamber setup for a cone penetration test (Lee et al. 2008).



Type of Boundary Conditions	Lateral Boundary Conditions	Top and Bottom Boundary Conditions
BC1	Constant Stress	Constant Stress
BC2	No displacement	No displacement
BC3	No displacement	Constant Stress
BC4	Constant Stress	No displacement

Fig. 2.4. Boundary condition types in calibration chamber tests (Salgado et al. 1998).

CHAPTER 3: DEVELOPMENT OF A MINIATURE CONE PENETROMETER

A schematic of the MCPT system is shown in Fig. 3.1, and a photograph of the constructed system is shown in Fig. 3.2. The MCPT combined five different components: (i) mini-piezocone, (ii) penetration system, (iii) calibration chamber, (iv) vertical loading system, and (v) data acquisition (DAQ) and control system. Design drawings of the calibration chamber and other components of the MCPT system are include in Appendix A.

3.1 Piezocone

A miniature piezocone with a diameter of 16 mm, 60° apex angle, and cone tip area of 2 cm² was used in this study (Fig. 3.3). A photograph of the mini-piezocone is shown in Fig. 3.4. During penetration of the mini-piezocone into the soil specimen, measurements of tip resistance, sleeve friction, and pore pressure were measured continuously with penetration via data logging equipment provided by the manufacturer of the mini-piezocone. The mini-piezocone (model NK003) was provided by Pagani Geotechnical Equipment.

3.2 Mini-Piezocone Penetration System

The mini-piezocone was pushed vertically downward into a soil specimen via a hydraulic cylinder attached to the top of the load frame (Fig. 3.1). The rate of penetration was controlled via a hydraulic fluid-filled reservoir and flow control valve. Hydraulic fluid within the reservoir was pressurized via air pressure, and the pressurized fluid was transferred into the hydraulic cylinder via the flow control valve.

The hydraulic cylinder had an inner diameter of 150 mm and stroke length of 300 mm. The diameter of the hydraulic cylinder was selected to meet anticipated reaction forces that corresponded to a maximum tip resistance of 20 MPa of the mini-piezocone. The stroke length of the hydraulic cylinder was selected to provide sufficient penetration into the calibration chamber.

Vertical displacement of the mini-piezocone during penetration was measured with a linear displacement transducer with capacity of 317 mm and accuracy of 0.25 % (Model SP1-25; TE Connectivity). A series of calibration tests were conducted to determine the range of displacement rates for the hydraulic system. The two variables evaluated were air pressure applied to the hydraulic reservoir and the opening position of the flow control valve (i.e., position ranged from 0-5, with 5 being the largest opening). Results of displacement rate versus air pressure applied to the hydraulic reservoir are shown in Fig. 3.5a. Displacement rates increased with opening on the flow control valve and with increased air pressure applied to the hydraulic reservoir. A second set of displacement rate calibration tests was conducted and the data are shown in Fig. 3.5b; essentially identical displacement rates were measured. Thus, potential displacement rates for the mini-piezocone in the MCPT system ranged from approximately 0.00001 mm/s to 0.72 mm/s.

3.3 Calibration Chamber

The calibration chamber was fabricated from PVC and had an inner diameter of 300 mm and height of 368 mm. A PVC end-cap was glued to the bottom of the pipe to create a watertight container. The calibration chamber yielded a chamber diameter to cone diameter ratio (D_c/d_c) of 19 and included rigid boundaries on all sides of the specimen (i.e., type BC3 boundary conditions in Fig. 2.4). The calibration chamber included two pore water pressure transducers located along the sidewall (Fig. 3.1) and a system to control vertical stress applied to a test specimen.

3.4 Vertical Loading System

The calibration chamber was placed on a load-cell platform situated on the base pedestal of a 50-kN load frame (ELE International Digital Tritest 50). The base pedestal of the load frame extended upwards to push the calibration chamber against a reaction plate to create stress on the surface of the specimen (Fig. 3.1). The reaction plate was fixed to the crossbar at the top of

the MCPT system via 25-mm-diameter threaded steel rods. Force generated via upward movement of the load frame was measured with a 44-kN pancake-style load cell fixed on a specially-designed load-cell platform that was situated between the load frame pedestal and calibration chamber. The load-cell platform included guide rods at each corner to help maintain vertical orientation between the load frame, calibration chamber, and mini-piezocone to avoid eccentric loading. The surface stress was used to consolidate the specimen to a known effective stress whereupon the mini-piezocone was then pushed into a soil specimen.

3.5 Data Acquisition and Control System

The DAQ and control system included a National Instrument (NI) USB-6215 DAQ board connected to a PC and controlled via LabVIEW software. This DAQ system recorded measurements of displacement of the base pedestal of the load frame, force from the load cell, displacement from the position transducer, and pore pressure from the two pore pressure transducers. Measurements were recorded every second and post-processed via a moving average in Microsoft Excel. In addition, a feedback control loop was written in the LabVIEW Program to control the vertical force applied to the surface of a specimen. This control program allowed a constant stress to be maintained on the surface of the specimen during consolidation and mini-piezocone penetration.

A digital DAQ system called TGAS08 was provided by Pagani Geotechnical Equipment to collect CPT test data. The TGAS08 plots real-time CPT measurements on the screen of the unit and recorded all data to be downloaded after each test. The mini-piezocone was calibrated by the manufacturer.

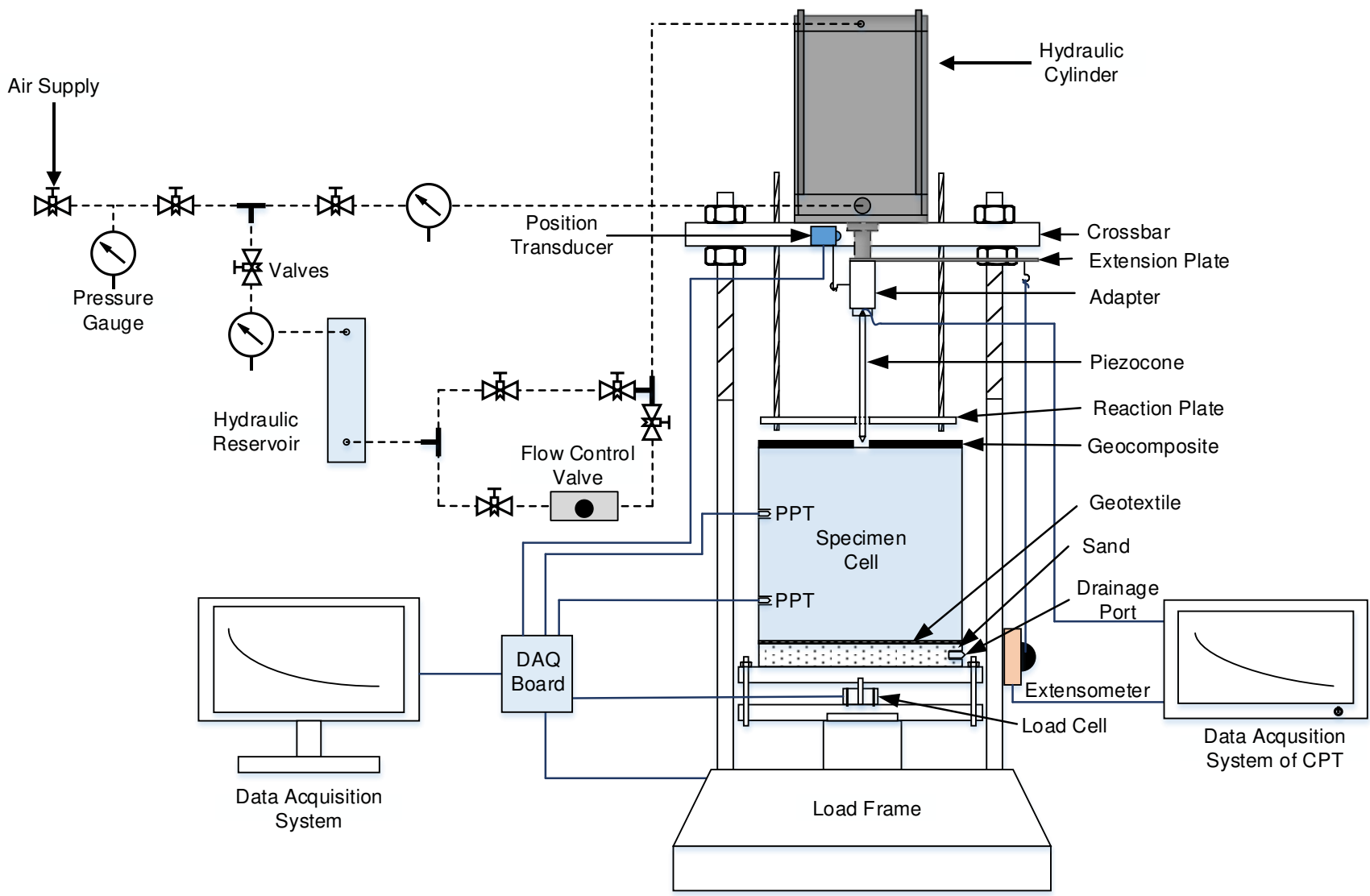


Fig. 3.1. Schematic of the miniature cone penetration test system (not to scale).

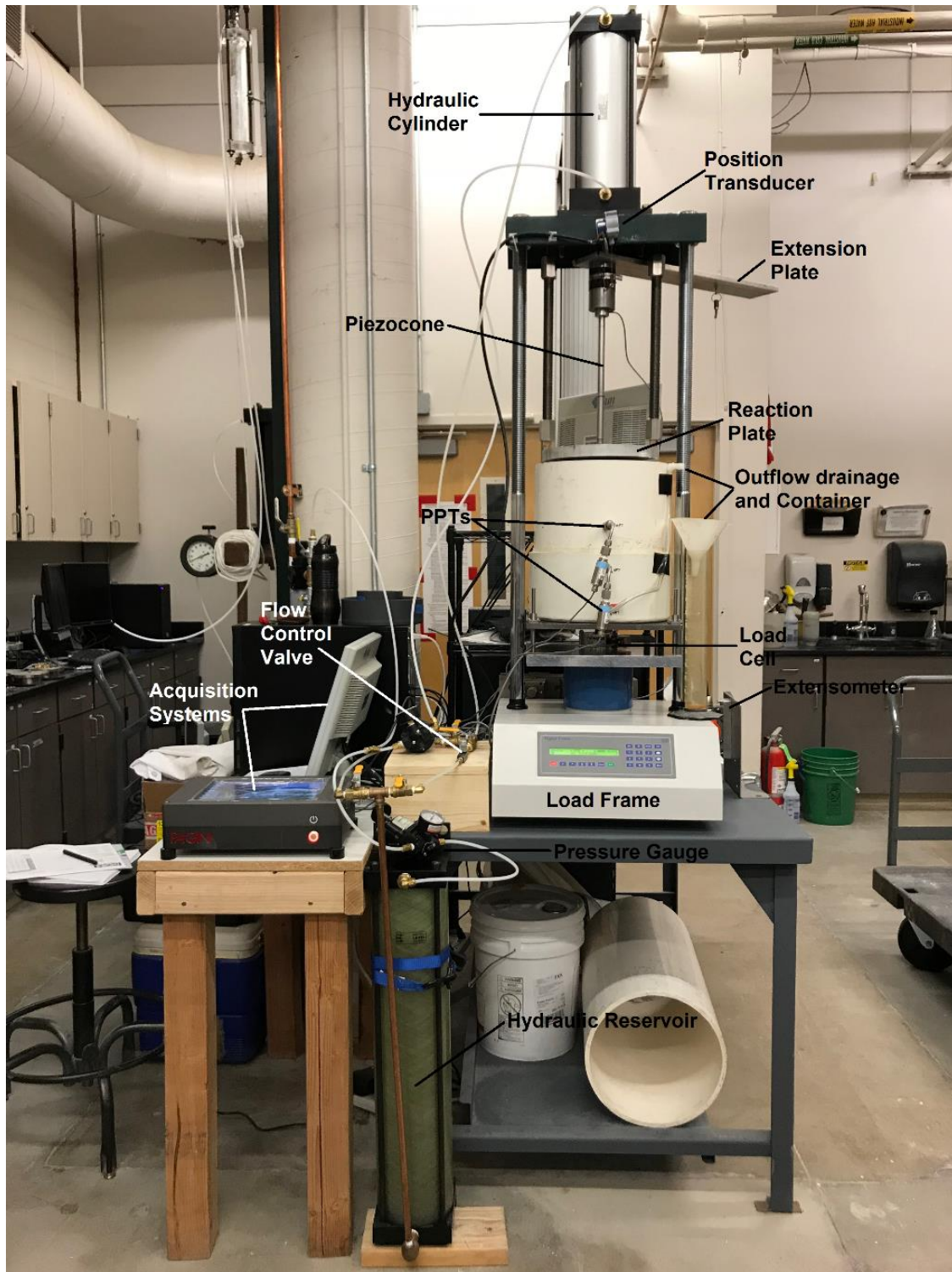


Fig. 3.2. Photograph of the miniature cone penetration test system.

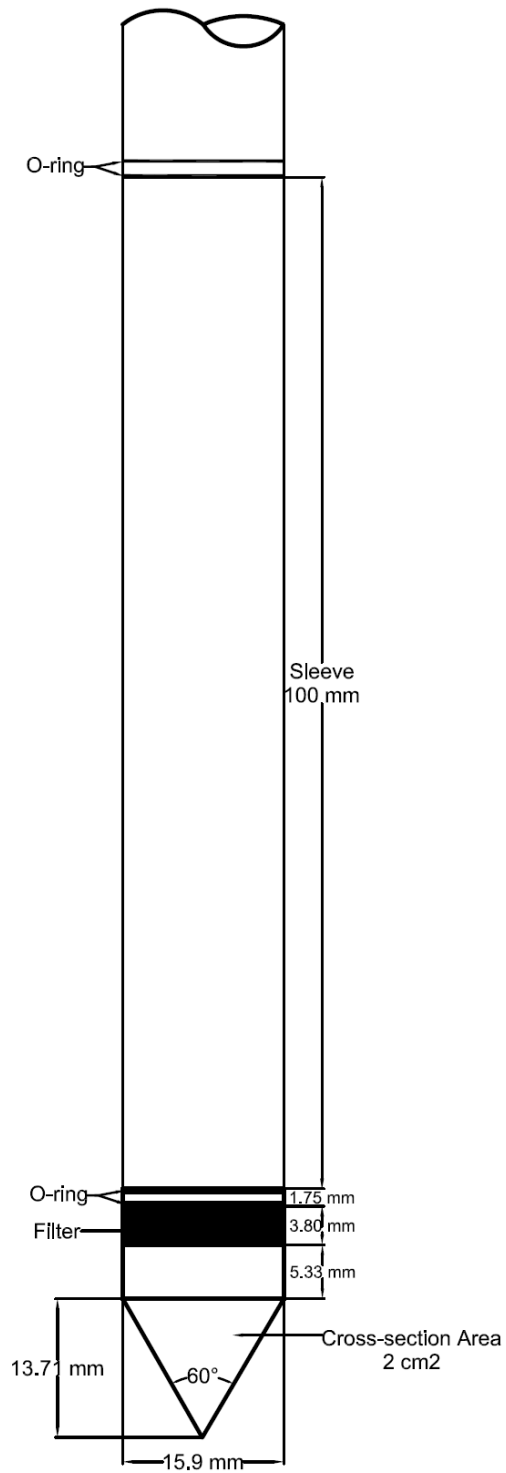


Fig. 3.3. Schematic of the miniature piezocone.

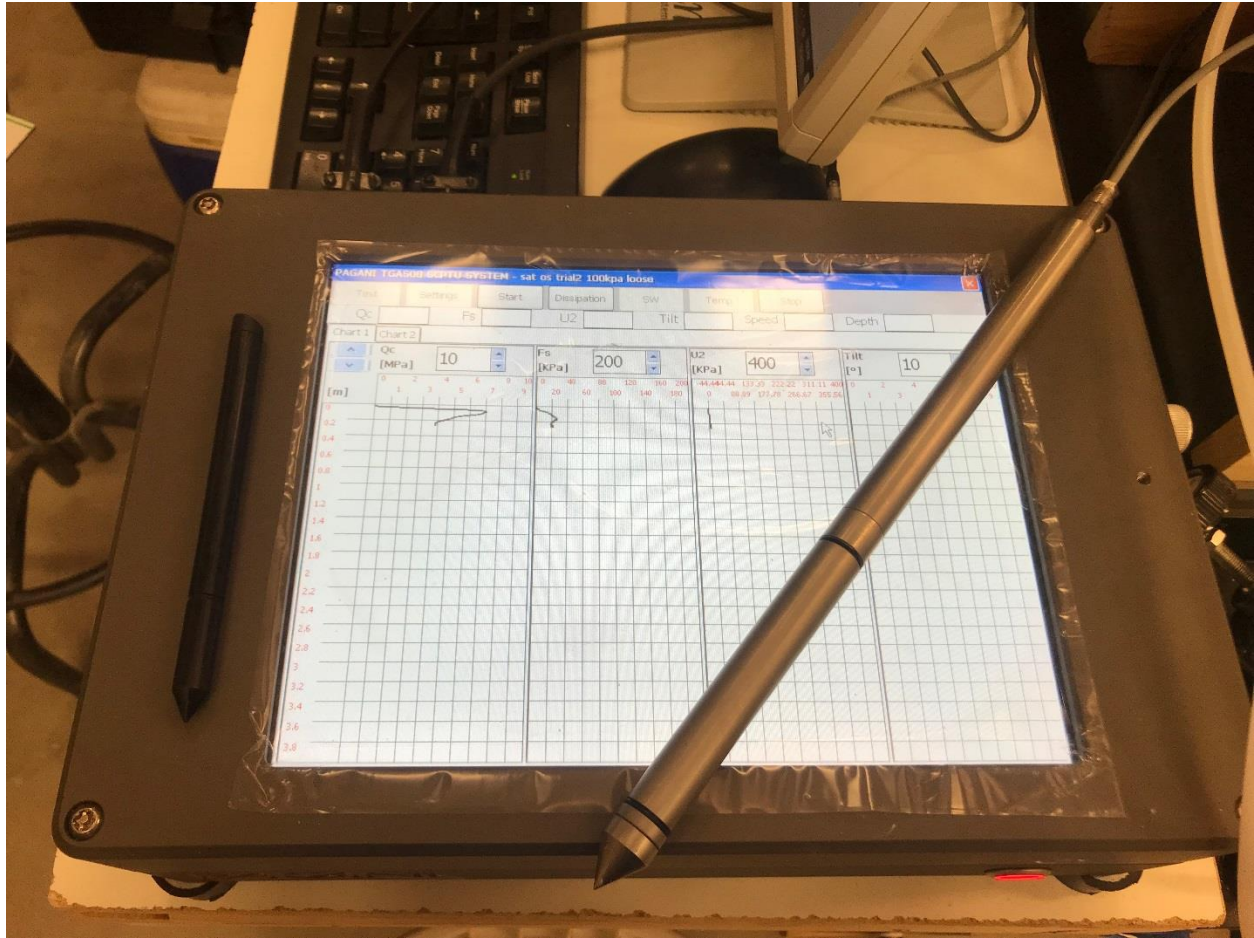


Fig. 3.4. Photograph of the mini-piezocone and DAQ system of CPT.

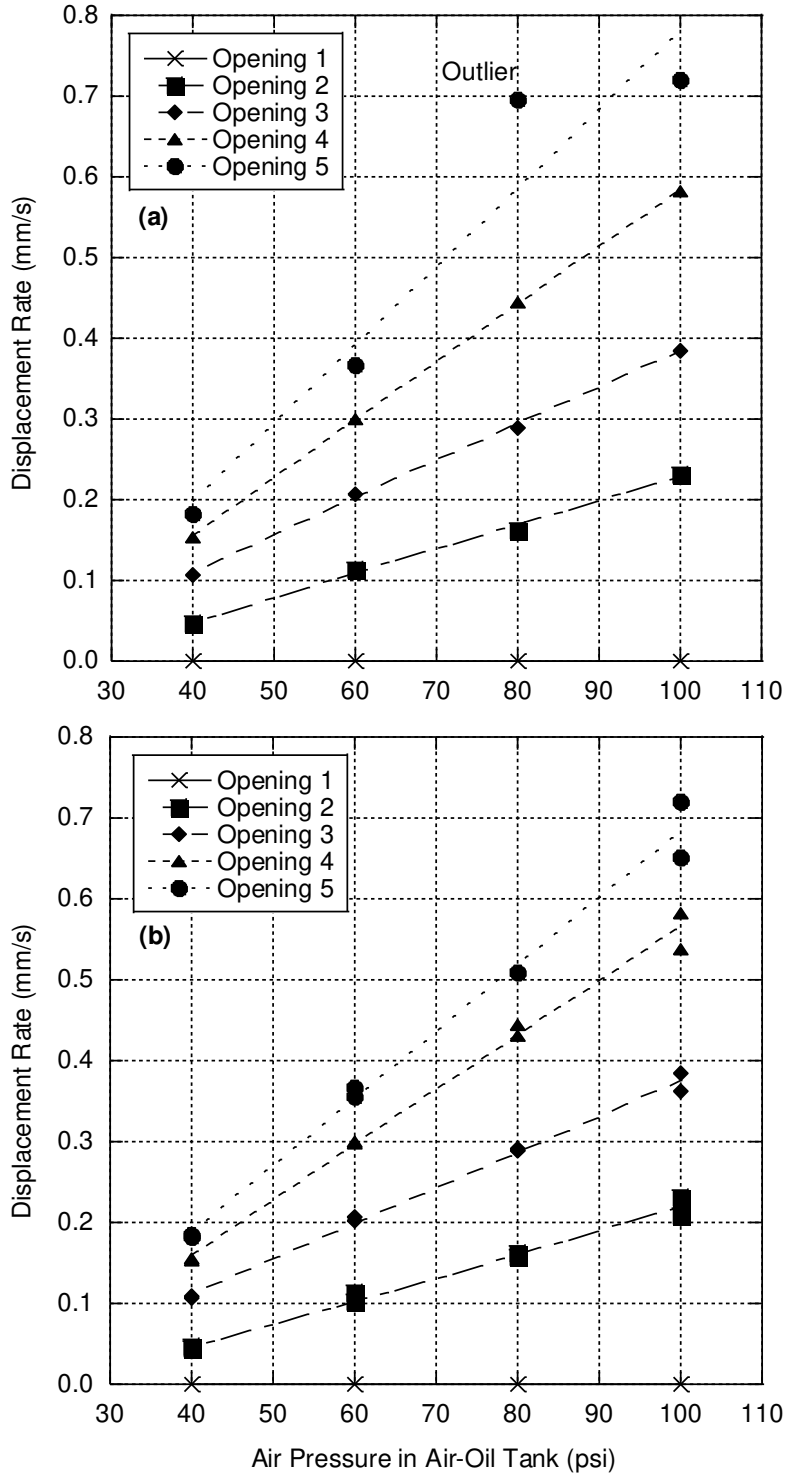


Fig. 3.5. Relationships of vertical displacement rate of the mini-piezocone versus air pressure applied to the hydraulic reservoir for two sets of experiments (a and b). The Opening refers to the position on the flow control valve, where 5 corresponds to the largest opening.

CHAPTER 4: MATERIALS AND METHOD

4.1 Materials

Three different materials were used in this study: (i) Ottawa sand, (ii) fine synthetic tailings (FST), and (iii) coal combustion product (CCP). Ottawa sand was used to verify the MCPT via comparison to results from previous mini-piezcone calibration chamber tests and to evaluate repeatability. Fine synthetic tailings were created from a mixture of kaolin clay and silica flour to compare strength properties determined via the MCPT to measurements made in consolidated undrained triaxial compression (Hamade, 2017). The CCP was obtained from a coal ash impoundment in North America and MCPT results were compared to shear strength determined for the same CCP in Herweynen (2018).

Geotechnical characteristics of the three materials are summarized in Table 4.1 and particle size distribution (PSD) curves are shown in Fig. 4.1. Ottawa sand was a poorly-graded clean sand with no fines that classified as SP according to Unified Soil Classification System (USCS) (ASTM D2487, 2017). Sand particles had a specific gravity (G_s) of 2.65 and a mean particle diameter (D_{50}) of 0.60 mm. The maximum void ratio (e_{max}) of Ottawa sand was determined according to ASTM D 4254 using a funnel to loosely place material, and the minimum void ratio (e_{min}) was measured according to ASTM D 4253; $e_{max} = 0.66$ and $e_{min} = 0.39$.

Geotechnical characteristics for FST were obtained from Hamade (2017), and geotechnical characteristics for CCP were obtained from Herweynen (2018). The FST was created as a mixture of 40% kaolin and 60% silica powder and classified as low plasticity clay (CL) based on a liquid limit (LL) of 37 and plasticity index (PI) of 15. In contrast, the CCP was predominantly silt-sized material and classified as low plasticity silt (ML) based on $LL = 41$ (BS 1377 method) and the plasticity limit being non-plastic (i.e., $PL = 0$). The G_s of FST was 2.63 and the G_s of CCP was 2.35 based on ASTM D854 (2014).

4.2 Miniature Cone Penetration Test (MCPT)

The MCPT was conducted in accordance with ASTM D3441 (2016) using equipment described in the previous chapter. The mini-piezocone used in this study had a projected cone area of 2 cm², friction sleeve area of 43 cm², and cone apex angle of 60°. The depth of the penetration for all experiments was approximately 250 mm.

The Ottawa sand specimens for the MCPT were prepared via wet pluviation. This method was conducted by slowly depositing sand particles into the calibration chamber that was filled with water to a specified depth. Sand particles were dropped from a height of approximately 10-mm above the water surface such that they settled individually to form the sand specimen. Wet pluviation was conducted in five layers of equal thickness (approximately 6 to 7 cm) to maintain an approximately constant depth of water for the sand particles to deposit. The height of each layer was measured via a digital caliper after pluviation of sand and the final height was computed to determine the initial void ratio (e_i) and initial relative density (Dr_i) of each specimen. Replicate Ottawa sand specimens were prepared at $e_i \approx 0.58, 0.62, \text{ and } 0.64$, which corresponded to $Dr_i = 29.0\%, 14.4\%, \text{ and } 10.0\%$, respectively. De-aired tap water was used in all specimens.

The FST and CCP specimens were prepared via slurry deposition by mixing de-aired tap water and air-dried material. The FST slurry was prepared at a solids content of 60%, whereas the CCP slurry was prepared at a solids content of 57%. The gravimetric water contents of FST and CCP were 66% and 75%, respectively. Slurries were mixed via a hand-held mixer to create a uniform slurry. Herweynen (2018) identified a minimum wait time of 48 h between specimen preparation and testing to allow for diagenesis to occur in the CCP. This 48-h wait time was adopted after consolidation was complete in a CCP specimen.

A schematic of the calibration chamber with test specimen is shown in Fig. 4.2. In all experiments, a 25-mm-thick layer of clean sand was compacted at the bottom of the cell to provide drainage and prevent clogging of the effluent port. A thin, non-woven geotextile was placed between the sand layer and slurry to provide separation. A geocomposite consisting of non-woven

geotextiles heat-bonded to a geonet, was placed on top of the slurry to provide separation and drainage. A hole was cut in the middle of the geocomposite to allow the mini-piezocone to pass through during testing. A layer of aluminum foil was placed over the hole during specimen consolidation to prevent material from squeezing out of the hole. The foil was easily ruptured by the mini-piezocone at the start of penetration.

The MCPT experiments on all materials were consolidated to a target vertical effective stress (σ'_v) prior to penetration. Ottawa sand specimens were consolidated under $\sigma'_v = 100$ kPa to evaluate repeatability and compare to literature. The CCP specimens were consolidated to $\sigma'_v = 40$ kPa and 88 kPa to compare to shear strength results (i.e., direct shear, triaxial compression, and vane shear) in Herweynen (2018). The FST specimens were consolidated to $\sigma'_v = 50$ kPa and 100 kPa to compare with triaxial compression test results in Hamade (2017).

The target σ'_v was applied instantaneously to the Ottawa sand specimens since this material drained rapidly and exhibited minor settlement. In contrast, an initial $\sigma'_v = 1$ kPa was applied on the FST and CCP specimens, and the magnitude of σ'_v was doubled incrementally as the specimen consolidated. Consolidation was deemed complete once excess pore pressure measured in the pore pressure transducers decreased, drainage from the bottom of the specimen ceased, and vertical displacement exhibited a change from primary to secondary consolidation. The pore water pressure and vertical deformation are plotted for each load increment that was induced by the load frame and plots are in Appendix B.

The final σ'_v was held constant for approximately 1 h after consolidation was complete. Subsequently, the final height was recorded to determine specimen density prior to penetration. Based on height changes in each load increment, relationships of $e-\sigma'_v$ from the tests on FST and CCP were developed and are shown in Appendix B (Fig. B.3 for FST and Fig. B.6 for CCP). According to these relationships, consolidation behavior of FST and CCP in the calibration chamber exhibited similar $e-\sigma'_v$ trends as measured other laboratory compression tests. Similar $e-\sigma'_v$ data suggests consistency in specimen preparation relative to the other studies used for

comparison (e.g., Hamade 2017; Herweynen 2018) and negligible development of side-wall friction in the calibration chamber.

According to ASTM D3441 (2016), the standard penetration rate for CPT is 20 mm/s, which corresponds to undrained conditions in clays and drained conditions in sands. Target penetration rates for the FST and CCP that correspond to drained and undrained conditions are summarized in Table 4.2. Based on the calculations in Table 4.2 and the potential displacement rates of the MCPT, CCP experiments were conducted with a penetration rate of 0.045 mm/s to achieve drained conditions, whereas FST experiments were conducted with a penetration rate of 0.2 mm/s to achieve undrained conditions. There was no concern regarding the rate of penetration in the Ottawa sand specimens since all rates would lead to drained conditions; thus, a rate of 0.36 mm/s was applied due to practicability of this rate in the apparatus.

Table 4.1 Geotechnical characteristics of the materials.

Properties/ Material	Ottawa Sand	FST	CCP
LL (%)	NA	37	41
PI (%)	NA	15	-
USCS	SP	CL	ML
d_{max} (mm)	9.5	0.05	2.00
Sand Content (%)	100	0	15
Silt Content (%)	0	58	83
Clay Content (%)	0	42	2
G_s	2.65	2.63	2.35
e_{min}	0.39	NA	NA
e_{max}	0.66	NA	NA
w_{opt} (%)	0	23	NA
γ_{dmax} (kN/m ³)	16.7	14.9	NA

Note: LL = liquid limit; PI = plasticity index (ASTM D4318); USCS = Unified Soil Classification System (ASTM D2487); d_{max} = maximum particle size (ASTM D422); G_s = specific gravity of solids (ASTM D854); w_{opt} = optimum water content and γ_{dmax} = maximum dry unit weight (ASTM D698); e_{min} and e_{max} = minimum and maximum void ratio (ASTM D 4253 and ASTM D4254); NA = not applicable. CCP data from Herweynen (2018) and FST data from Hamade (2017).

Table 4.2 Penetration rates of the specimens based on the drainage conditions.

Specimen	σ'_v (kPa)	c_v (mm ² /s)	d_c (mm)	V_{un}	V_d	v_{un} (mm/s)	v_d (mm/s)
CCP		145	16	10	0.05	9.0	0.045
FST	2.0	0.26	16	10	0.05	0.16	0.0008
	3.5	0.14	16	10	0.05	0.088	0.0004
	7.9	0.16	16	10	0.05	0.098	0.0005
	15	0.11	16	10	0.05	0.066	0.0003
	30	0.20	16	10	0.05	0.13	0.0006
	61	0.32	16	10	0.05	0.20	0.0009
	126	0.21	16	10	0.05	0.13	0.0007

Note: σ'_v = effective vertical stress, c_v = coefficient of consolidation, d_c = cone diameter, V_{un} = normalized penetration rate for undrained conditions, V_d = normalized penetration rate for drained conditions, v_{un} = penetration rate for undrained condition, and v_d = penetration rate for drained condition. Values of V are from Kim et al. (2008), c_v of CCP from Herweyneyen (2018), and c_v and σ'_v for FST were from Tian (2017).

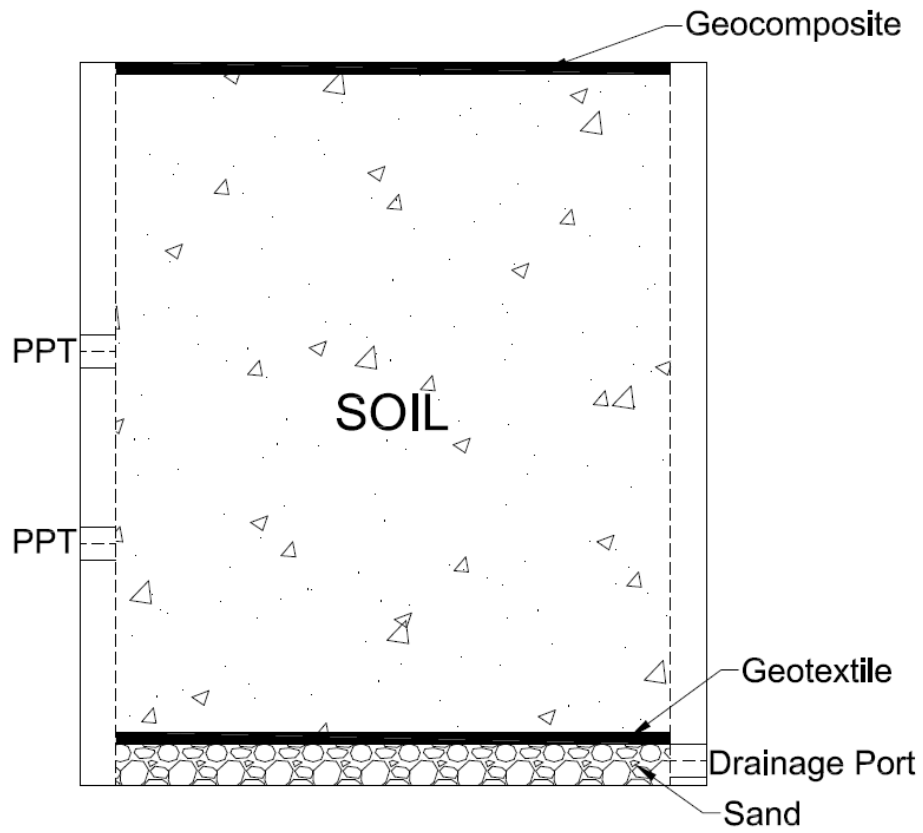


Fig. 4.2. Schematic of the calibration chamber and specimen boundaries for the fine synthetic tailings and coal combustion product.

CHAPTER 5: RESULTS AND DISCUSSION

A total of 10 MCPTs were conducted for this study; six tests on Ottawa sand, two tests on FST, and two tests on CCP. The Ottawa sand specimens were penetrated at an approximate rate of 0.36 mm/s since there was negligible concern with development of excess pore water pressure. The penetration rate for the MCPTs on CCP was 0.045 mm/s, which was selected to achieve drained conditions. In contrast, the penetration rate for the MCPTs on FST was 0.2 mm/s, which was selected to achieve undrained conditions.

5.1 MCPT Measurements on Ottawa Sand

A summary of the MCPTs conducted on Ottawa sand is in Table 5.1 and includes σ'_v , initial relative density of the specimen (Dr_i), final relative density after consolidation (Dr_f) under σ'_v , q_c , f_s , and R_f . The penetration resistances (q_c , f_s) and R_f values tabulated in Table 5.1 are averages from MCPT measurements recorded between depths of 17 and 26 cm. In this depth range, the entire mini-piezcone was within the sand specimens and measurements of q_c and f_s were approximately constant (described subsequently).

Repeatability of the MCPT method was evaluated via duplicate tests on Ottawa sand consolidated to three different Dr_f under $\sigma'_v = 100$ kPa. Results from the six MCPTs on Ottawa sand penetrated at $Dr_f \approx 24\%$, 29% , and 43% are shown in Figs. 5.1, 5.2, and 5.3, respectively. The MCPT results include q_c , f_s , and R_f as a function of depth. The q_c calculated and plotted in Figs. 5.1 – 5.3 accounted for the effect of excess pore water pressure acting on unequal cone areas. However, the influence of pore pressure on tip resistance was negligible since very low excess pore water pressure developed during cone penetration. Therefore, the q_c values of Ottawa sand specimens were equal to q_t values.

The q_c and f_s measurements on Ottawa sand specimens exhibited similar characteristics as a function of depth for the three relative densities. A peak q_c developed between depths of

approximately 7 and 13 cm, whereupon q_c decreased and stabilized with continuous penetration. In contrast, f_s increased from the start of penetration to a depth of 10 to 15 cm and then remained approximately constant with continuous penetration. These relationships document the changing state of shear resistance measured by the mini-piezocone during penetration.

The length of the friction sleeve on the mini-piezocone was 100 mm and the full functional length of the mini-piezocone from tip to end of the frictional sleeve was approximately 125 mm (Fig. 3.3). Thus, the entire friction sleeve was not fully mobilized within a test specimen until the tip of the mini-piezocone penetrated to depth of 12.5 cm within the specimen (i.e., approximately 14.5 cm depth in Figs. 5.1, 5.2, and 5.3). Shear resistance of a soil specimen measured by the mini-piezocone was a combination of q_c and f_s . Thus, an increasing f_s during initial penetration represents a continuous increase in mobilized frictional resistance as the friction sleeve penetrated into the specimen. The peak q_c represents a point where the balance of shear resistance between q_c and f_s shifted and began to equilibrate to what were representative q_c and f_s when the friction sleeve was completely within a test specimen.

Sleeve friction measured in all of the MCPTs on Ottawa sand reached a maximum value around 15 cm of depth and then remained essentially constant with subsequent penetration (Figs. 5.1, 5.2, and 5.3). Once sleeve friction reached a nearly constant value around 15 cm of depth, tip resistance also remained essentially constant with continuous penetration. The one caveat was MCPTs on the loosest sand specimens ($Dr_f \approx 24\%$ in Fig. 5.1), where peak q_c decreased between 15 cm and 20 cm of depth before remaining constant. Regardless of this minor difference, q_c and f_s trends as a function of depth in the calibration chamber were similar for MCPTs and explainable based on mobilization of shear resistance acting on tip and along the sleeve of the mini-piezocone.

The q_c , f_s , and R_f data from all MCPTs conducted on Ottawa sand are replotted in Fig. 5.4 as a function of normalized specimen depth, which is equivalent to penetration depth within a specimen divided by specimen thickness. The line labeled as “100% friction mobilized” in Fig. 5.4

corresponds to a depth of 12.5 cm within a specimen, which was the depth when the entire friction sleeve was within a specimen. Values of q_c , f_s , and R_f from the depth corresponding to complete mobilized frictional resistance to the final measurements at a normalized specimen depth of 0.8 were nearly constant. Furthermore, values in the normalized specimen depth range of 0.5 to 0.8 corresponds to depths of 17 and 26 cm as plotted in Figs. 5.1 – 5.3. An average q_c and f_s were computed for each Ottawa sand specimen in the depth range of 17 to 26 cm to represent shear resistance of the mini-piezocone for a given MCPT (Table 5.1).

5.1.1 The Effect of Increase in Relative Density on q_c and f_s

Relationships between the average q_c and f_s (Table 5.1) as a function of Dr_f from the MCPTs on Ottawa sand are shown in Fig. 5.5. An increase in q_c and f_s was observed with an increase in Dr_f for Ottawa sand tested under $\sigma'_v = 100$ kPa. Linear regression lines were added to the data sets to document the positive correlations, and both regression lines had coefficients of determination (R^2) ≥ 0.97 . The regression lines are unique to the Ottawa sand used in the MCPTs as well as the stress and boundary conditions imposed in the calibration chamber.

The relationship between q_c and relative density from MCPTs in this study are replotted in Fig. 5.6 along with results from Damavandi-Monfared and Sadrekarimi (2015). The q_c values from Damavandi-Monfared and Sadrekarimi (2015) were obtained with a 6-mm-diameter mini-piezocone on Ottawa sand consolidated under $\sigma'_v = 100$ kPa. The Ottawa sand used in their experiments was a poorly graded clean sand composed of rounded to sub-angular quartz particles with $d_{50} = 0.19$ mm. Similar positive correlations between q_c and relative density and similar magnitudes of q_c were observed in both studies.

The D_c/d_c ratio between the calibration chamber and mini-piezocone used in Damavandi-Monfared and Sadrekarimi (2015) was 25, which was slightly larger than $D_c/d_c = 19$ in this study. In clean sands, q_c has been reported to increase with a decrease in D_c/d_c due to influence of the boundaries that can interfere with the zone of shear deformation developed during cone

penetration (Ghionna and Jamiolkowski 1991). In addition, Ottawa sand in this study had $d_{50} = 0.60$ mm, whereby the increase in particle size may also have contributed to higher q_c . Thus, the higher q_c in this study relative to Damavandi-Monfared and Sadrekarimi (2015) may have developed from the different D_c/d_c and/or physical characteristics of the sand. Regardless of these differences, similarity in q_c trends and magnitudes between the two studies support the MCPT methodology developed herein.

A relationship between normalized cone tip resistance and relative density from the MCPTs in this study are shown in Fig. 5.7 that are superimposed on results from Jamiolkowski et al. (2001) and Mayne (2006). Jamiolkowski et al. (2001) evaluated 456 unique calibration chamber data sets on normally consolidated sand. Each data set was corrected for boundary size effects to develop the relationship shown in Fig. 5.7. Data in Fig. 5.7 for undisturbed sands were from CPT results reported in Mayne (2006), and both laboratory calibration chamber data and field data define the same positive trend between relative density and normalized cone resistance. Data from this study align with both positive correlations in Fig. 5.7 and further support accuracy of the tip resistance measurements obtained from the MCPT system developed in this study.

5.1.2 Soil Behavior Type

Robertson (1990) presented a modified classification chart that yields anticipated soil composition and soil behavior based on normalized results from CPT. The modified classification chart is shown in Fig. 5.8 and data points from the six MCPTs conducted on Ottawa sand are plotted on the chart. The soil behavior summarized in Fig. 5.8 is an apparent response of the soil to CPT (Mayne 2007), whereby Zones 6 and 7 correspond to drained penetration and Zones 1, 2, 3, and 4 correspond to undrained penetration. Soil behavior in Zones 5, 8, and 9 may exhibit partially drained behavior during penetration. The MCPTs conducted on Ottawa sand plot in Zone 6 (sands – clean sand to silty sand) and along the boundary with Zone 5 (sand mixtures – silty sand to sandy silt). The MCPT results were in agreement with the large CPT database used by

Robertson (1990) to compile the soil behavior plot. This agreement further supports the MCPT methodology and cone resistance parameters (q_c and f_s) measured via the mini-piezcone.

5.1.3 Friction Angle

Relationships between ϕ' of Ottawa sand specimens and normalized cone resistance are shown in Fig. 5.9. Empirical models are included in Fig. 5.9 from Kulhawy and Mayne (1990) and Uzielli et al. (2013) based on statistical analyses of corrected calibration chamber data, and data from Mayne (2014) represent comparisons between in situ CPTs and triaxial strength tests on exhumed sand from each CPT site. Friction angles were estimated for the MCPTs in this study based on Eq. 2.8, which is the empirical relationship shown as Kulhawy and Mayne (1990) in Fig. 5.9. Thus, ϕ' ranges between 36° and 38° as predicted from normalized cone resistance.

A compilation of ϕ' for Ottawa sand and corresponding relative densities reported in previous studies is in Table 5.2. This compilation indicates that ϕ' of Ottawa sand ranges between 25° and 43° for relative density ranging from 4% to 82%. The ϕ' predicted based on MCPT results correspond to relative densities between 24.2% to 43.4%. Therefore, ϕ' predicted based on the MCPT yielded a range (36° and 38°) that was comparable to what would be anticipated based on literature. Additional material specific strength testing would be the next step to make more direct comparisons to ϕ' predicted based on MCPT.

5.2 MCPT Measurements on FST and CCP

A summary of the MCPTs conducted on FST and CCP is in Table 5.3. Included in Table 5.3 is a summary of the average corrected cone tip resistance (q_t), f_s , and pore water pressure (u_2) for each MCPT as well as predictions of undrained shear strength (S_u) for FST and predictions of ϕ' for CCP. Relationships of q_t , f_s , and u_2 as a function of depth for the MCPTs on FST are shown in Figs. 5.10 and 5.11 and on CCP are shown in Figs. 5.12 and 5.13. Cone tip resistance was computed as corrected cone resistance since pore water pressure developed in each of the

MCPTs and was used to correct q_c for pore pressure acting on unequal areas of the cone. Corrections were made via Eq. 2.7 and the net area ratio of the piezocone (a) was 0.75.

5.2.1 Penetration Behavior of FST

The q_t response as a function of depth for the two MCPTs on FST was similar. The q_t was negligible within the first few centimeters of specimen penetration, increased to a peak around a depth of 5 cm, was approximately constant between depths of 10 to 17 cm, and then increased continuously with subsequent penetration as the mini-piezocone approached the bottom of the specimens (Figs. 5.10 and 5.11). The negligible q_t within the first few centimeters of specimen penetration was attributed to limited consolidation beneath the hole in the load plate that permitted the mini-piezocone to pass through. The peak q_t and subsequent decrease were likely due to a change in shear resistance as the tip of the mini-piezocone penetrated and an increasing amount of the shaft developed frictional resistance. Complete penetration of the mini-piezocone coincided with a depth of 15 cm in Figs. 5.10 and 5.11, and the measurements made between approximately 15 cm and 17 cm were taken as representative of the shear strength of the FST in the MCPT. The subsequent increase in q_t coincided with a continuous decrease in f_s , which was attributed to influence from the bottom boundary (described subsequently).

In contrast to the undulating response of q_t and f_s as a function of depth in the FST specimens, pore pressure increased and remained nearly constant with depth. Pore pressure was measured at the filter on the mini-piezocone, which was positioned approximately 20 mm from the cone tip (Fig. 3.3). Thus, more than 2 cm of specimen penetration were required to bring the filter in contact with a given specimen. This lag response of the filter penetrating into a specimen was observed as positive pore pressure beginning to increase at a depth of 5 cm, which coincided with an actual depth of penetration in the specimen of 3 cm. Once the filter on the mini-piezocone was completely within an FST specimen, pore pressure rapidly increased and then remained essentially constant after reaching a depth of 10-12 cm. The pore pressure response

was positive in both FST specimens, and larger in the specimen consolidated to $\sigma'_v = 100$ kPa (Fig. 5.11) relative to $\sigma'_v = 50$ kPa (Fig. 5.10). This response is typical of normally consolidated clayey materials and agreed with pore pressure generated during consolidated undrained triaxial compression tests conducted on FST by Hamade (2017).

5.2.2 Penetration Behavior of CCP

The q_t response as a function of depth for the two MCPTs on CCP was also similar. A negligible to low q_t was measured within the first few centimeters of specimen penetration, which subsequently increased, remained nearly constant, and then increased as the mini-piezocone approached the bottom of the specimen (Figs. 5.12 and 5.13). Complete penetration of the mini-piezocone to engage the full friction sleeve was achieved at approximately 15 cm of depth, and at this point of penetration in both CCP specimens, q_t was constant and remained constant until a penetration depth of approximately 17 cm. The q_t in the range of 15-17 cm were taken as representative of the specimen density and stress conditions.

The trend of f_s as a function of depth was such that f_s increased continuously with cone penetration and then leveled off near the end of the experiment. The f_s was approximately constant for the CCP tests at $\sigma'_v = 40$ kPa for the depth range of 15-17 cm, which coincided with full penetration of the mini-piezocone and constant q_t (Fig. 5.12). The f_s of the CCP test at $\sigma'_v = 88$ kPa did not stop increasing until penetration had reached a depth of 18 cm, which coincided with the increasing trend in q_t attributed to interference between the mini-piezocone and bottom boundary (Fig. 5.13). Thus, for the CCP at $\sigma'_v = 88$ kPa, an average f_s was computed from the depth range of 15-17 cm when q_t was constant and the friction sleeve was fully mobilized.

A positive pore pressure response was measured during the MCPTs on CCP (Figs. 5.12 and 5.13). The general shape of the pore pressure responses were similar to FSTs, whereby negligible pore pressure was measured at the start of penetration that was followed by an increase with increasing penetration depth to reach a nearly constant magnitude. However, the magnitude

of positive pore pressures measured in the CCP were one to two orders of magnitude lower than the FST.

5.2.3 MCPT Comparison

All data from the MCPTs on FST and CCP were re-plotted with respect to normalized specimen depth as shown in Fig. 5.14. The overall comparison of q_t indicates that an increase in σ'_v for a given material produced an increase in q_t , and furthermore, higher q_t were measured for the CCP relative to the FST. These comparisons were anticipated as the sandy/silty composition of the CCP has higher shear strength relative to FST for normally consolidated materials under similar σ'_v .

The horizontal gray bar in Fig. 5.14 identifies a depth range when full penetration of the mini-piezocone was achieved such that 100% mobilized frictional resistance developed along the friction sleeve. Each of the q_t relationships for the FST and CCP specimens exhibit an increase in q_t for normalized specimen depths ≥ 0.70 . At this penetration, there was only 60-70 mm of specimen remaining between the tip of the piezocone and bottom surface of the specimen. The similarity in all of the increasing q_t relationships suggests that there was an effect from the bottom boundary on measured tip resistance as the probe approached the bottom boundary. At a similar magnitude of normalized specimen depth (0.70) in the Ottawa sand specimens, approximately 100 mm of specimen remained between the tip of the piezocone and bottom boundary, and at full penetration (normalized depth ~ 0.8) nearly 60 mm remained beneath the cone tip. Although not directly evaluated in this study, the bottom boundary appears to influence q_t measured in the MCPT as the piezocone approached the bottom boundary.

Relationships of pore water pressure in the MCPTs as a function of normalized specimen depth are shown for all three materials in Fig. 5.15. The pore pressure response from four of the six tests on Ottawa sand are shown on different scales in Fig. 5.15a and 5.15b. The data in Fig. 5.15a indicate that small positive pore pressures, ranging from approximately 0 to 2 kPa above

static pore pressure, were measured in the Ottawa sand specimens. This magnitude of pore pressure is shown in Fig. 5.15b on the same scale as the FST and CCP in Fig. 5.15c. Visual comparison of the pore pressure trends suggest similar pore pressure response between Ottawa sand and CCP, based on low excess pore pressure and close comparison to static levels. In contrast, positive pore pressures measured in FST were considerably larger than the Ottawa sand and CCP. Although positive pore pressures were measured in all three materials, the low pore pressures in Ottawa sand and CCP suggest that these materials experienced drained conditions during cone penetration, whereas the large positive pore pressures in FST indicate that FST experienced undrained conditions.

5.2.4 Undrained Shear Strength Assessment of FST

Undrained shear strength (S_u) was estimated for FST based on the MCPTs and are tabulated in Table 5.3. The MCPT data for FST show pronounced positive pore pressure generated during penetration, which was an indication that FST experienced undrained shear behavior. The S_u was determined via Eq. 2.12 based on $\sigma_{v0} = \sigma'_v = 100$ kPa and $N_{kt} = 10$ as recommended by Lunne et al. (1997) for normally consolidated clayey materials. The $S_u = 13$ kPa for FST consolidated to $\sigma'_v = 50$ kPa and $S_u = 35$ kPa for σ'_v consolidated to 100 kPa.

Hamade (2017) conducted consolidated undrained triaxial tests on FST. Comparisons between S_u versus mean effective stress (p') at the end of consolidation for triaxial tests in Hamade (2017) and MCPTs conducted in this study are shown in Fig. 5.16. The p' for both sets of data represents the effective stress state present in the soil specimens and prior to shear in triaxial compression or prior to penetration in the MCPTs. A linear regression line was fit to data from Hamade (2017) and forced through the origin, which captures the increase in S_u as a function of increasing p' . The S_u estimated from MCPTs on FST show a similar increasing trend with increasing p' at the end of consolidation. Although the data set on FST from the MCPTs is limited to two points, both measurements of S_u agree with the magnitude and trend that would be

anticipated based on triaxial testing. This comparison of S_u suggests that the MCPT system developed herein can yield accurate estimates of undrained shear strength for fine-grained clayey materials prepared from slurry.

5.2.5 Effective Stress Friction Angle Assessment of CCP

The ϕ' for CCP based on MCPT were estimated via Eq. 2.8 and are summarized in Table 5.3. The average ϕ' estimated for the CCP specimen consolidated to $\sigma'_v = 40$ kPa was 28.7° and ϕ' estimated for the CCP specimen consolidated to $\sigma'_v = 88$ kPa was 30.4° . Herweyner (2018) conducted consolidated undrained triaxial tests on CCP for a range of effective consolidation stress of 10 to 100 kPa and reported a range of $\phi' = 31.8^\circ$ to 36.4° , with a single composite $\phi' = 36^\circ$ that was representative of the drained strength envelope. The ϕ' estimated from the MCPTs appear to underestimate ϕ' from triaxial compression and can be taken as a conservative estimate of ϕ' .

5.3 Practical Implications

The MCPT system described herein was designed with the objective of creating a calibration chamber that coupled with a mini-piezocone to evaluate soft, fine-grained soils prepared from slurry. In general, the evaluation of three different materials (i.e., loose sand, fine-synthetic tailings, and coal combustion product) in the MCPT suggests shear behavior assessed via mini-piezocone penetration was explainable based on material composition and penetration rate. Furthermore, tip resistance and sleeve friction measurements from the MCPT yielded accurate estimates of soil shear strength. Additional refinement of the testing method and data analysis combined with additional testing of slurry-prepared materials will further improve the experimental approach.

The main practical implications of the MCPT system relate to (i) verification of the mini-piezocone and (ii) development of empirical relationships for slurry-prepared soils. Calibration

chamber testing is necessary to assess newly developed equipment (e.g., miniature piezocones) and the MCPT system developed herein incorporated a commercially-available mini-piezocone for which limited data currently exist. The testing conducted herein lends support to the ability of this mini-piezocone to yield relevant measurements of tip resistance, sleeve friction, and pore water pressure. A key subsequent step for assessing the mini-piezocone will be to conduct side-by-side assessments with larger CPTs to provide additional confidence to practicing engineers that the mini-piezocone is an in situ tool they can rely on. The mini-piezocone will require a much lower reaction force in the field, which should make the mini-piezocone advantageous for in situ testing of slurry materials that have limited strength.

The second key practical implication of the MCPT system is the ability to use the system to develop empirical relationships for industry by-products and mine wastes that have not been well characterized by CPT (e.g., coal combustion product). Field application of the mini-piezocone in, for example, a coal ash impoundment, requires that empirical relationships are available to correlate measurements from the mini-piezocone to estimates of shear strength. Data presented herein suggest the MCPT system can yield accurate estimates of undrained shear strength and perhaps slight underestimates of effective stress friction angles for slurry-prepared soils. After subsequent refinement of the MCPT system, the system should provide the ability to create design curves for the mini-piezocone in engineering practice.

Table 5.1 Summary of miniature cone penetration tests conducted on Ottawa sand.

Test No	σ'_v (kPa)	Dr_i (%)	Dr_f (%)	q_c (MPa)	f_s (kPa)	R_f (%)
1	100	9.30	24.20	4.39 ± 0.09	19.24 ± 0.59	0.44 ± 0.01
1R	100	10.00	24.90	4.76 ± 0.17	19.71 ± 1.15	0.41 ± 0.02
2	100	14.00	28.80	5.17 ± 0.15	20.89 ± 1.41	0.40 ± 0.03
2R	100	14.40	29.20	5.34 ± 0.03	23.18 ± 1.62	0.44 ± 0.03
3	100	28.90	43.30	6.45 ± 0.08	34.40 ± 1.39	0.53 ± 0.02
3R	100	29.00	43.40	6.50 ± 0.16	34.50 ± 1.57	0.53 ± 0.03

Notes: R = repeated experiments; σ'_v = vertical effective stress; Dr_i = relative density before consolidation; Dr_f = relative density after consolidation; q_c = cone tip resistance; f_s = sleeve friction; R_f = friction ratio

Table 5.2 Comparison between internal effective stress friction angles of Ottawa sand reported in literature and friction angles predicted based on miniature cone penetration tests in this study.

Researches	Relative Density (%)	Effective Friction Angle (°)
Lambrechts and Leonards (1978)	57	32
Salgado et al. (2000)	27-81	30 - 37
Schmertmann (1978)	20-80	28 - 43
Sherif et al. (1974)	4-73	25 - 42.7
Veismanis (1974)	20-73	33 - 41
Current Study	24.2	35.7
	24.9	36.1
	28.8	36.4
	29.2	36.6
	43.3	37.5
	43.4	37.5

Table 5.3 Summary of miniature cone penetration tests conducted on fine synthetic tailings (FST) and coal combustion product (CCP), and estimated shear strength for each material.

Specimen	σ'_v (kPa)	e_i	e_f	q_t (MPa)	f_s (kPa)	u_2 (kPa)	S_u (kPa)	ϕ'
FST	50	1.75	0.85	0.03	3.00	67.7	13	—
	100	1.72	0.89	0.12	6.26	109.1	35	—
CCP	40	1.77	1.05	0.65	6.79	4.2	—	28.7
	88	1.73	1.07	1.37	7.82	7.4	—	30.4

Note: σ'_v = vertical effective stress; e_i = initial void ratio; e_f = final void ratio; q_c = cone tip resistance; f_s = sleeve friction; u_2 = pore water pressure behind the cone tip; S_u = undrained shear strength; ϕ' = estimated effective friction angle

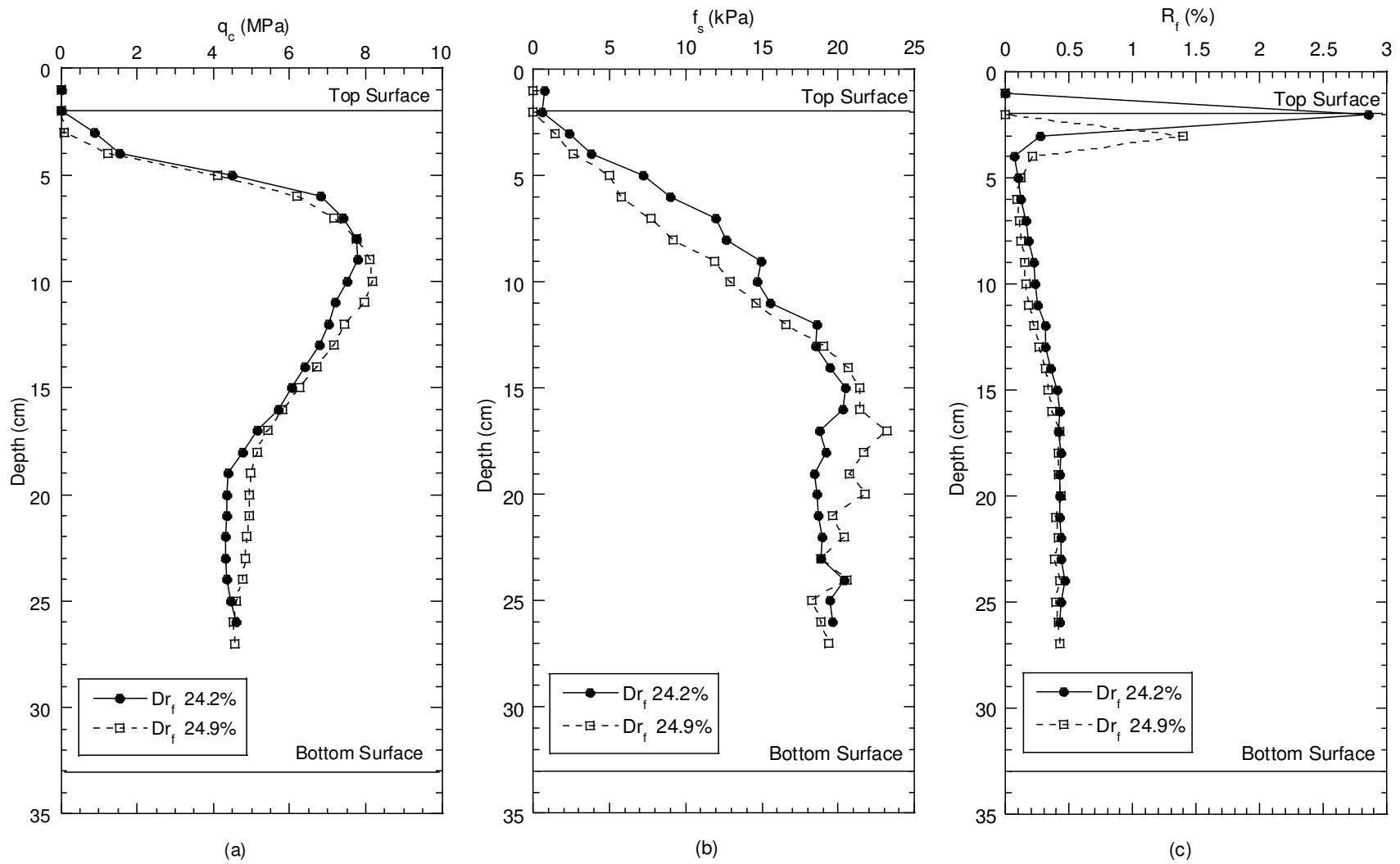


Fig. 5.1. Relationships of (a) tip resistance (q_c), (b) sleeve friction (f_s), and (c) friction ratio (R_f) as a function of penetration depth for miniature cone penetration tests on Ottawa sand at final relative densities (Dr_f) \approx 24%.

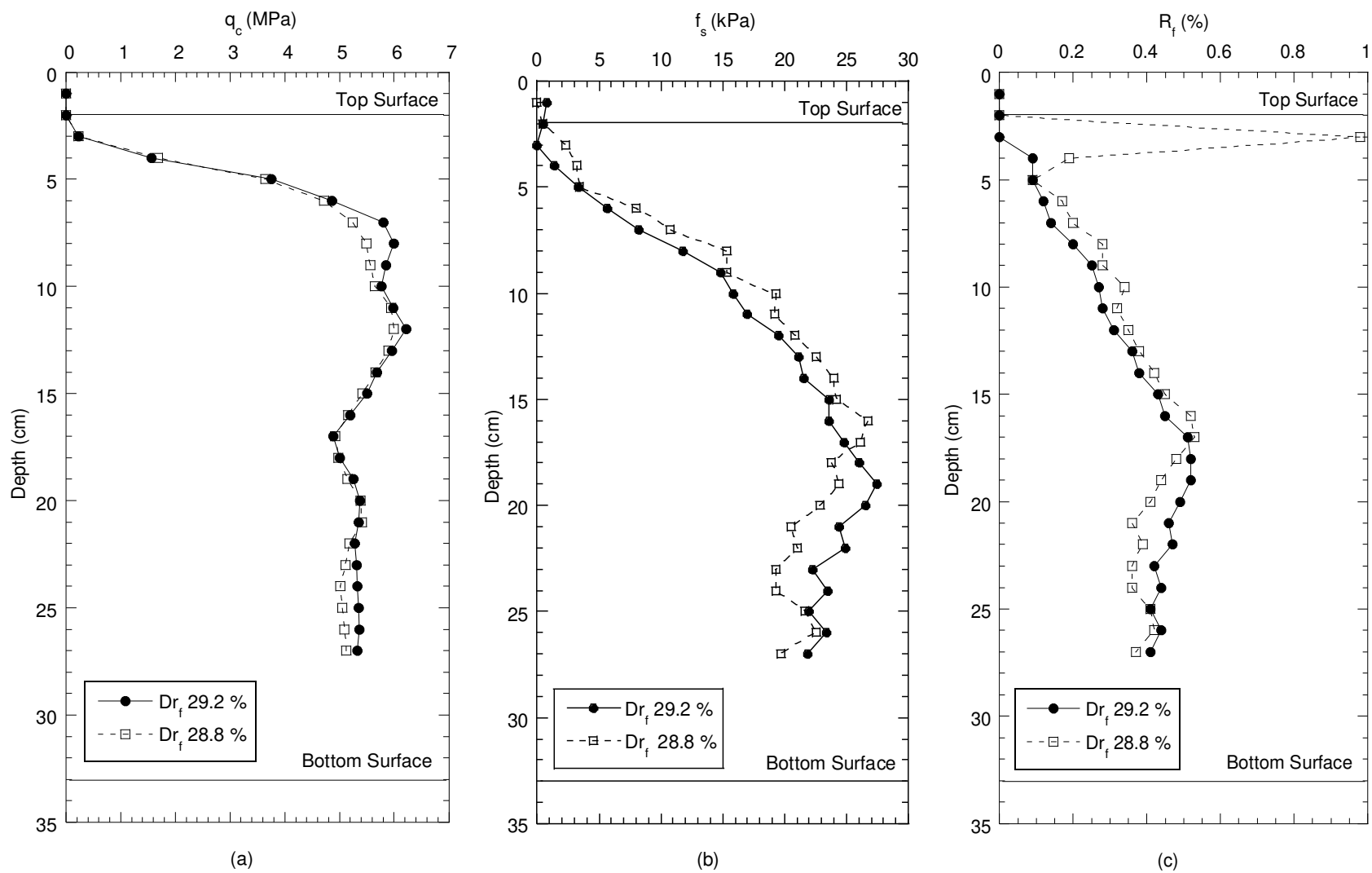


Fig. 5.2. Relationships of (a) tip resistance (q_c), (b) sleeve friction (f_s), and (c) friction ratio (R_f) as a function of penetration depth for miniature cone penetration tests on Ottawa sand at final relative densities (Dr_f) \approx 29%.

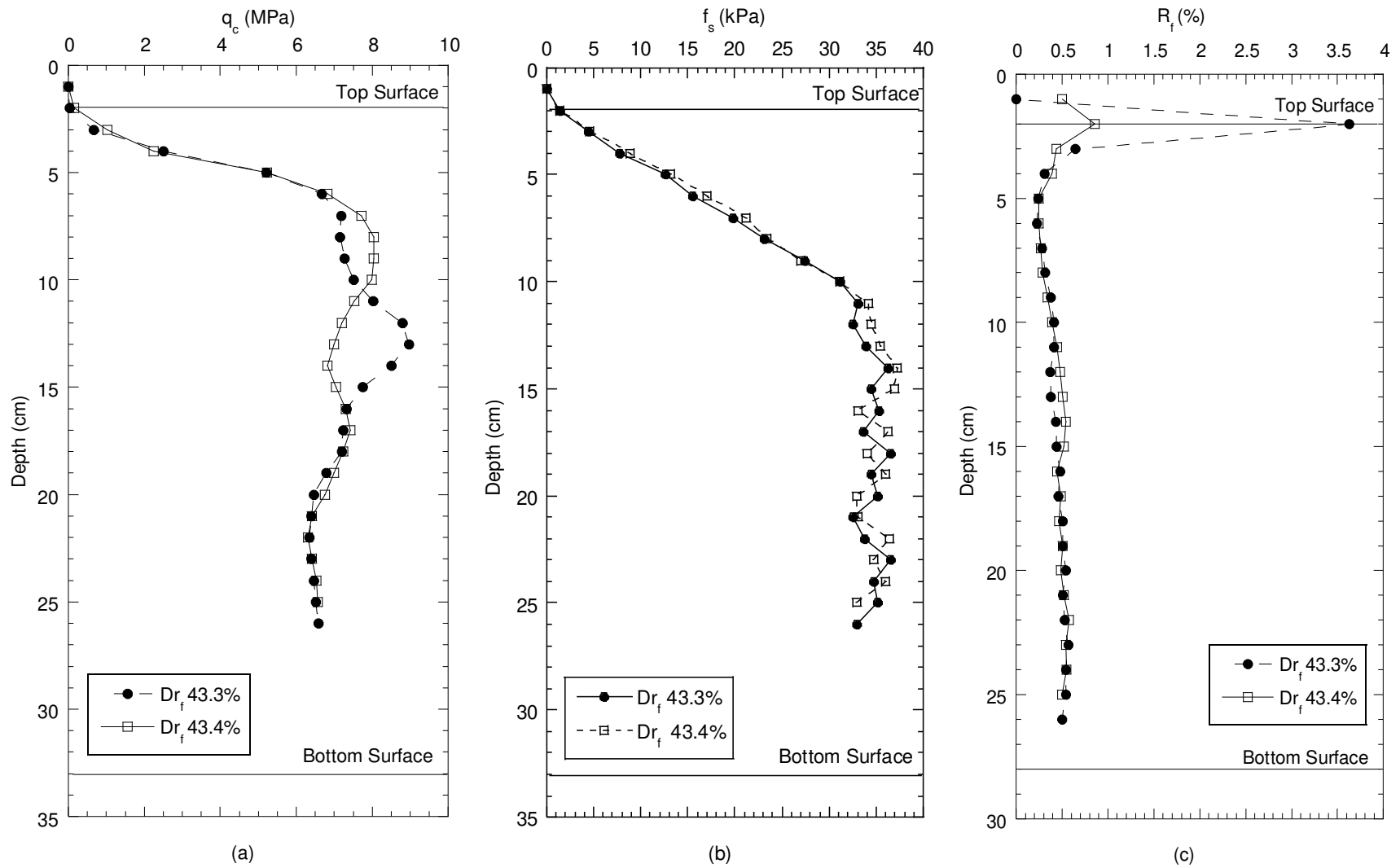


Fig. 5.3. Relationships of (a) tip resistance (q_c), (b) sleeve friction (f_s), and (c) friction ratio (R_f) as a function of penetration depth for miniature cone penetration tests on Ottawa sand at final relative densities (Dr_f) \approx 43%.

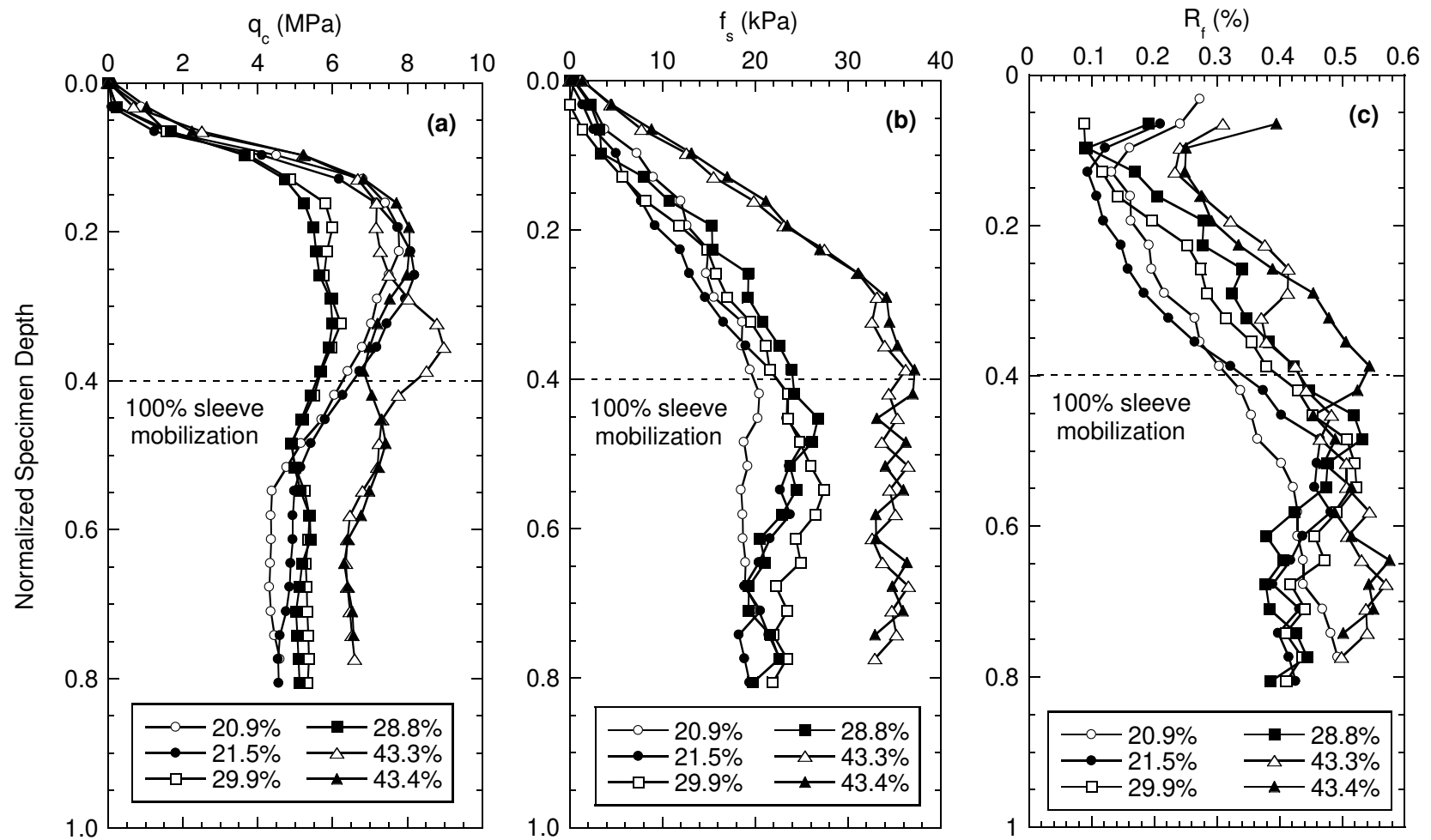


Fig. 5.4. Relationships of (a) tip resistance (q_c), (b) sleeve friction (f_s), and (c) friction ratio (R_f) as a function of normalized specimen depth for all six miniature cone penetration tests on Ottawa sand. Normalized specimen depth = penetration depth below specimen surface / specimen thickness. Final relative densities (D_r) listed in the legend.

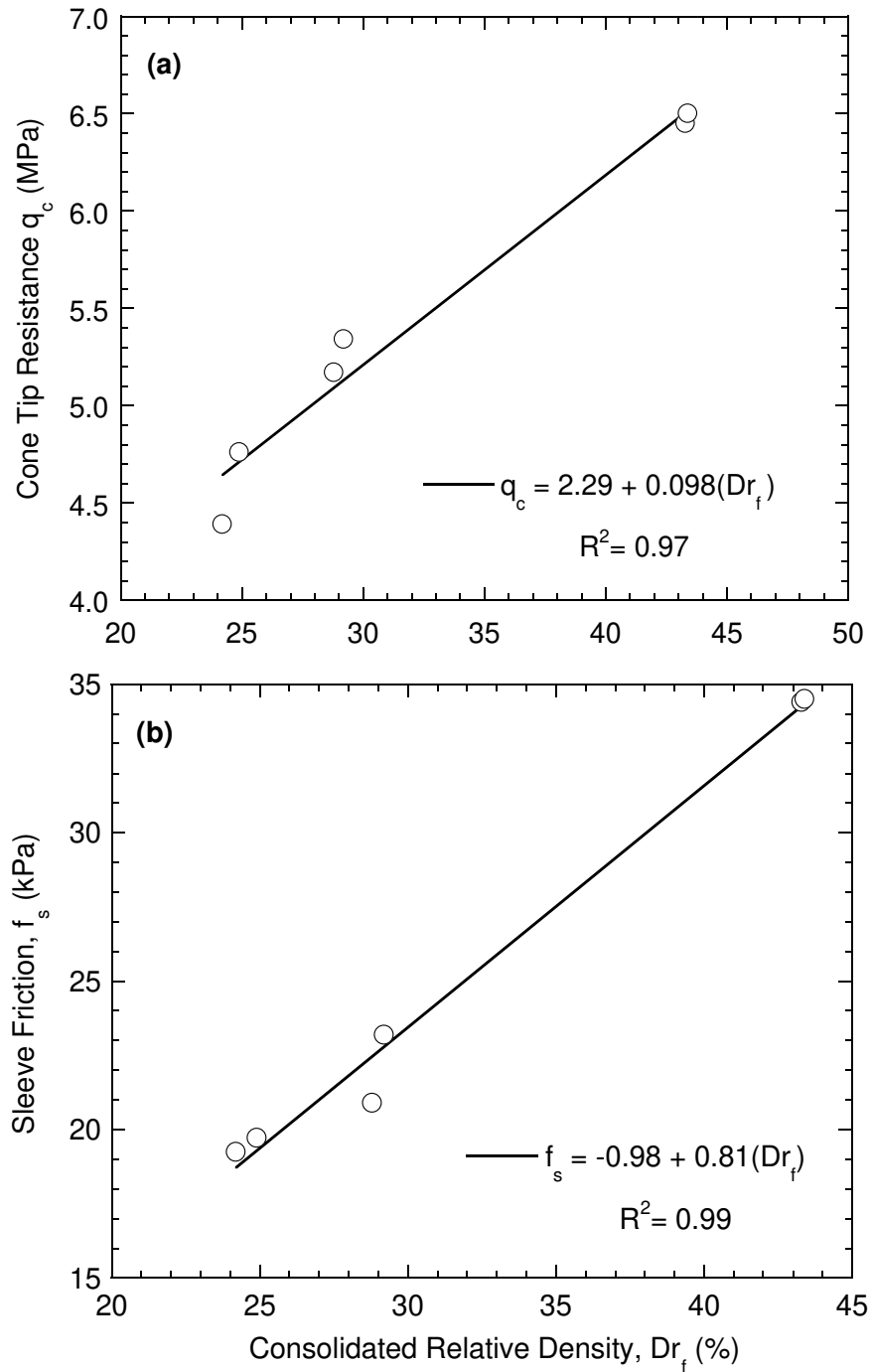


Fig. 5.5. Relationships of (a) tip resistance and (b) sleeve friction versus consolidated relative density of the Ottawa sand specimens.

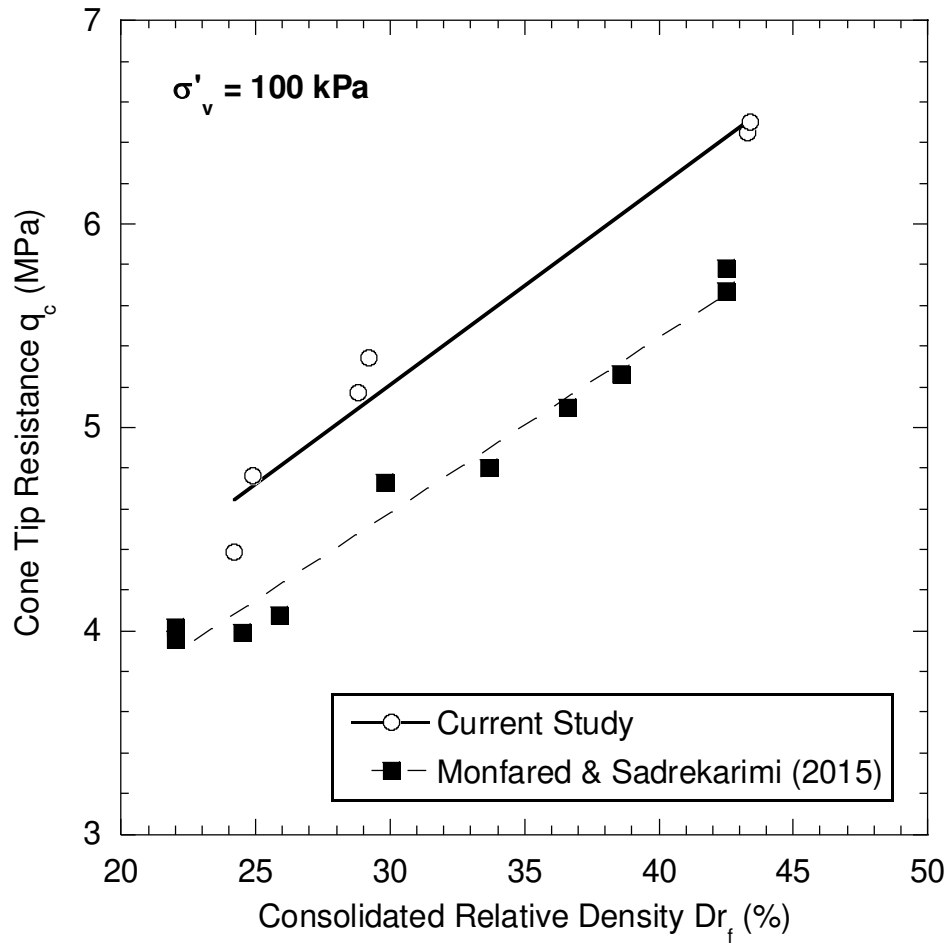


Fig. 5.6. Comparison of cone tip resistance versus consolidated relative density relationships from miniature cone penetration tests on Ottawa sand conducted in this study and in Damavandi-Monfared and Sadrekarimi (2015). All tests were conducted for sand consolidated under a vertical effective stress (σ'_v) of 100 kPa.

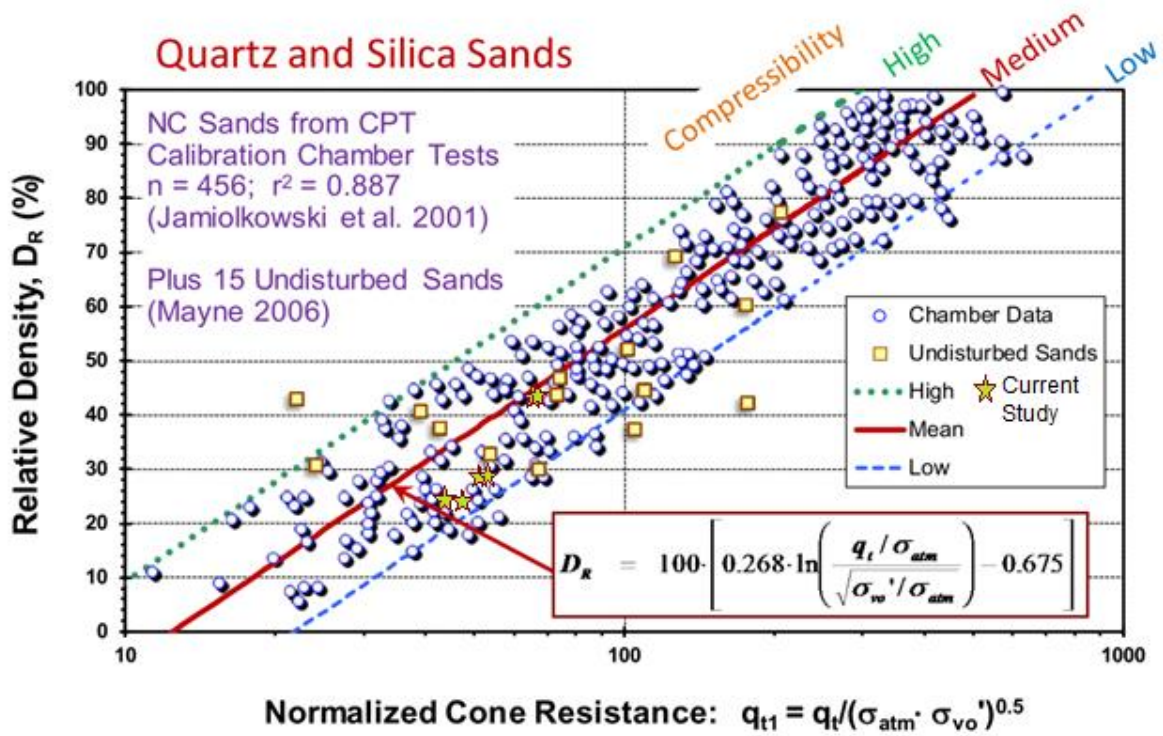
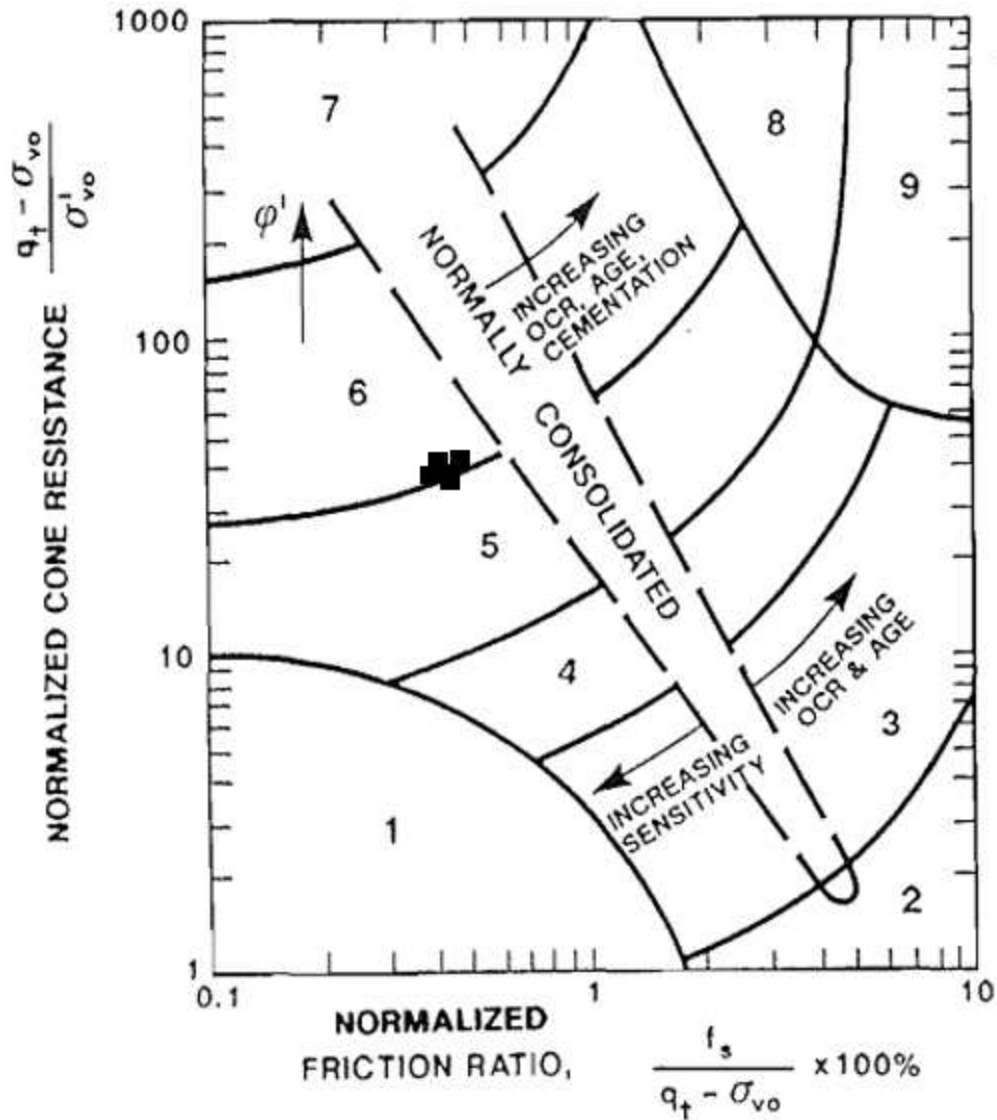


Fig. 5.7. Comparison of q_{t1} values from MCPT experiments of this study with other experiments conducted by Mayne (2006).



- | | |
|--|-------------------------------------|
| 1. SENSITIVE, FINE GRAINED | 6. SANDS – CLEAN SAND TO SILTY SAND |
| 2. ORGANIC SOILS – PEATS | 7. GRAVELLY SAND TO SAND |
| 3. CLAYS – CLAY TO SILTY CLAY | 8. VERY STIFF SAND TO CLAYEY* SAND |
| 4. SILT MIXTURES – CLAYEY SILT TO SILTY CLAY | 9. VERY STIFF, FINE GRAINED* |
| 5. SAND MIXTURES – SILTY SAND TO SANDY SILT | |

(*) HEAVILY OVERCONSOLIDATED OR CEMENTED

Fig. 5.8. Relationship of normalized tip resistance versus normalized friction ratio from Robertson (1990) that includes soil identification zones based on cone penetration test results. Data from the miniature cone penetration tests conducted in this study on Ottawa sand are plotted as black squares.

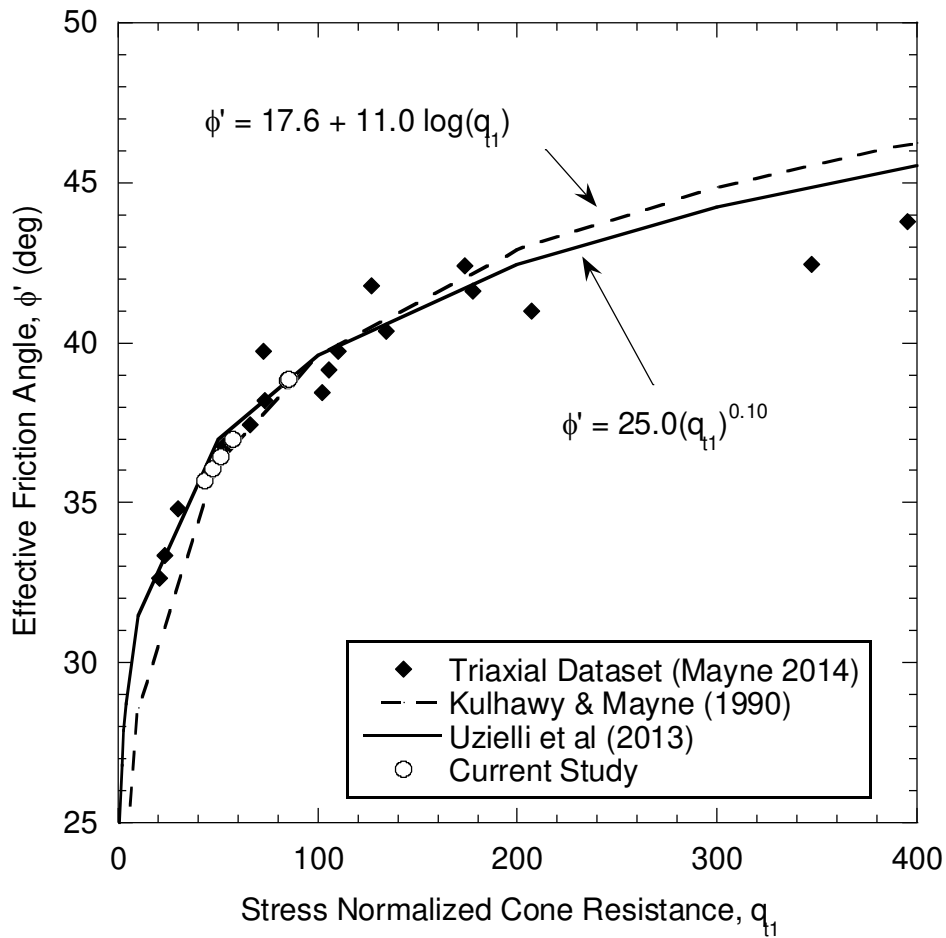


Fig. 5.9. Compilation of triaxial data and empirical relationships on clean Ottawa sands between the effective friction angle (ϕ') and normalized cone resistance from a cone penetration test. Normalized cone resistances from miniature cone penetration tests in this study were used to estimate ϕ' based on the relationship in Kulhawy and Mayne (1990).

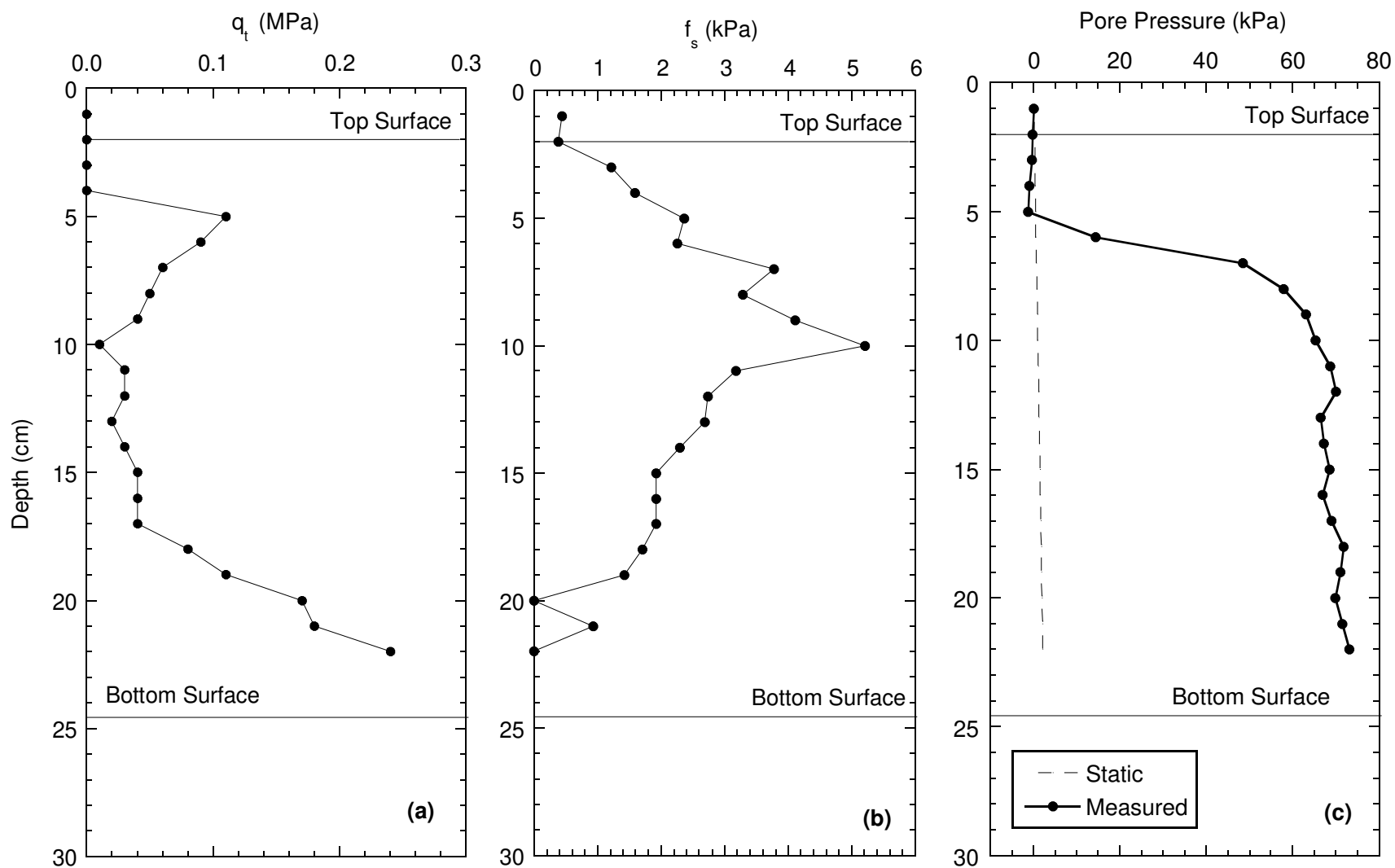


Fig. 5.10. Relationships of (a) tip resistance (q_c), (b) sleeve friction (f_s), and (c) pore water pressure as a function of penetration depth for the miniature cone penetration test on FST consolidated under a vertical effective stress (σ'_v) of 50 kPa.

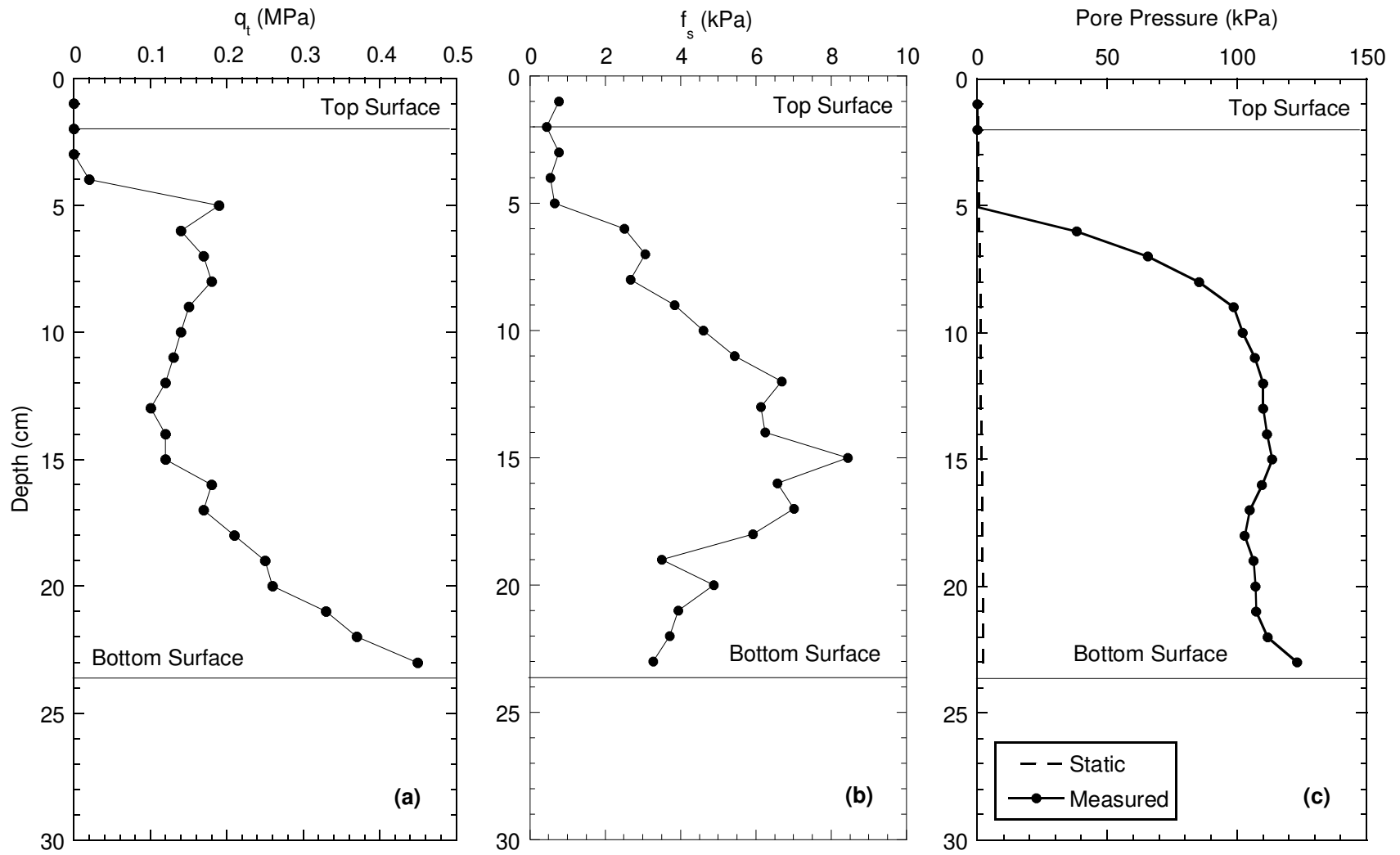


Fig. 5.11. Relationships of (a) tip resistance (q_c), (b) sleeve friction (f_s), and (c) pore water pressure as a function of penetration depth for the miniature cone penetration test on FST consolidated under a vertical effective stress (σ'_v) of 100 kPa.

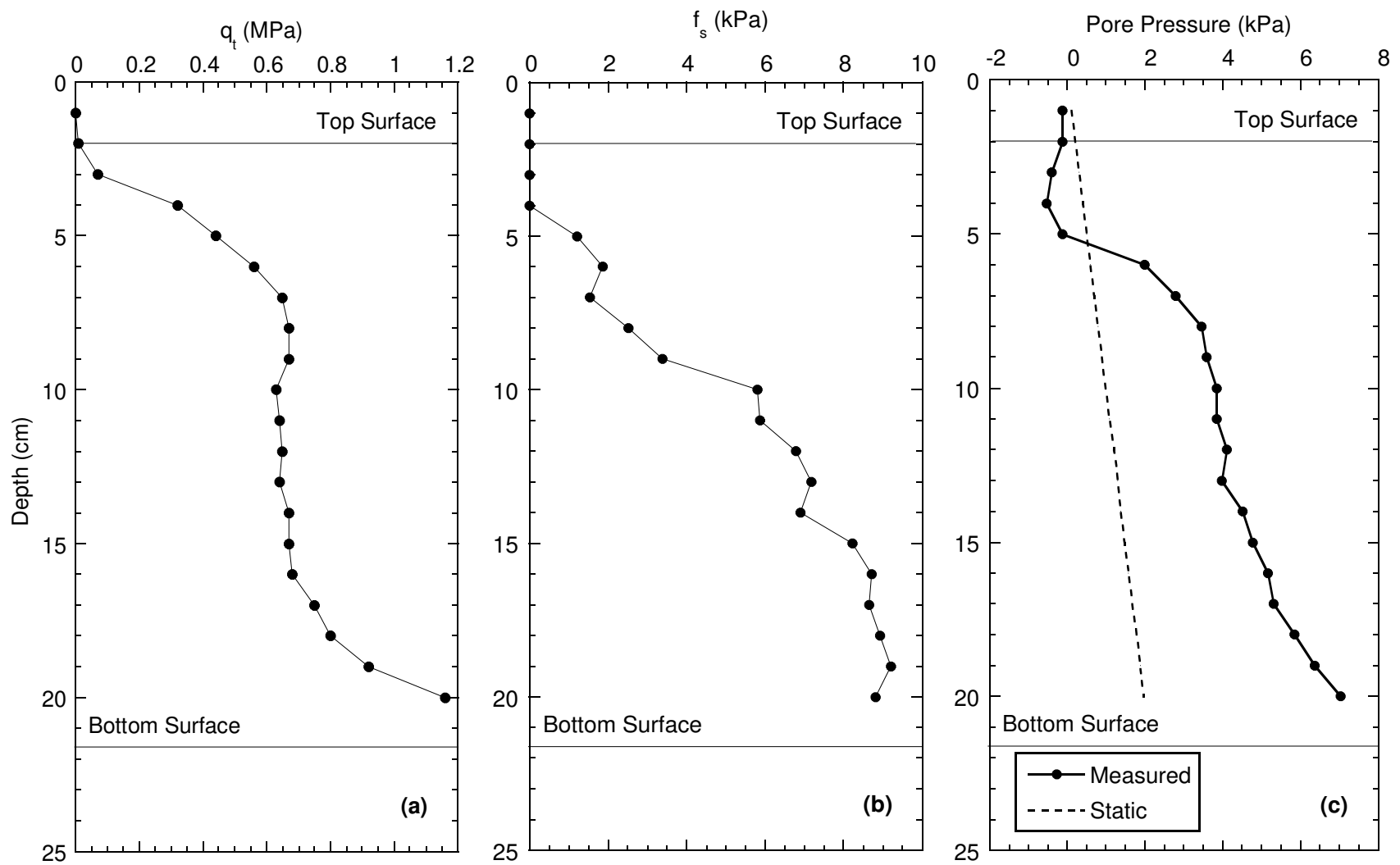
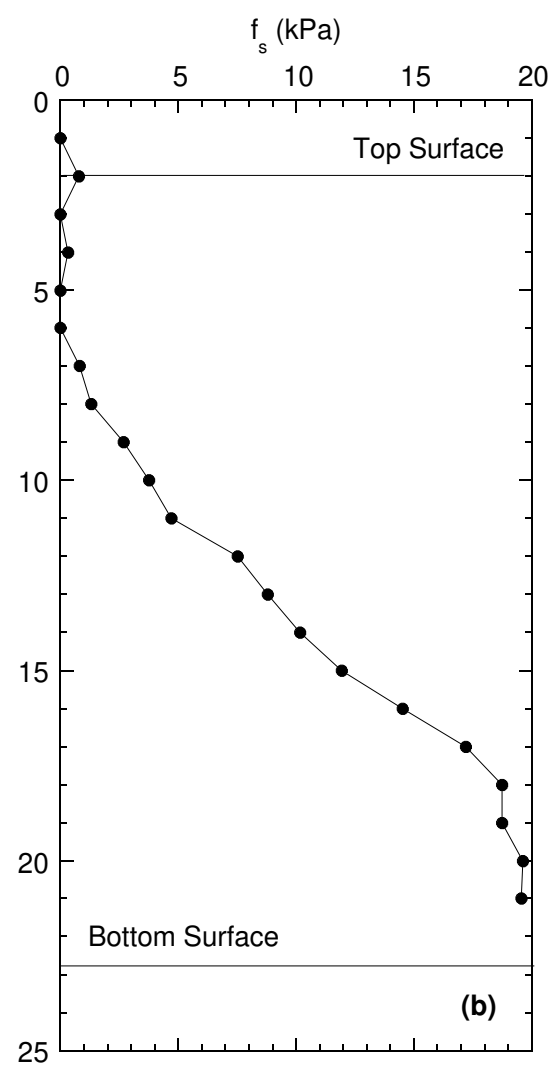
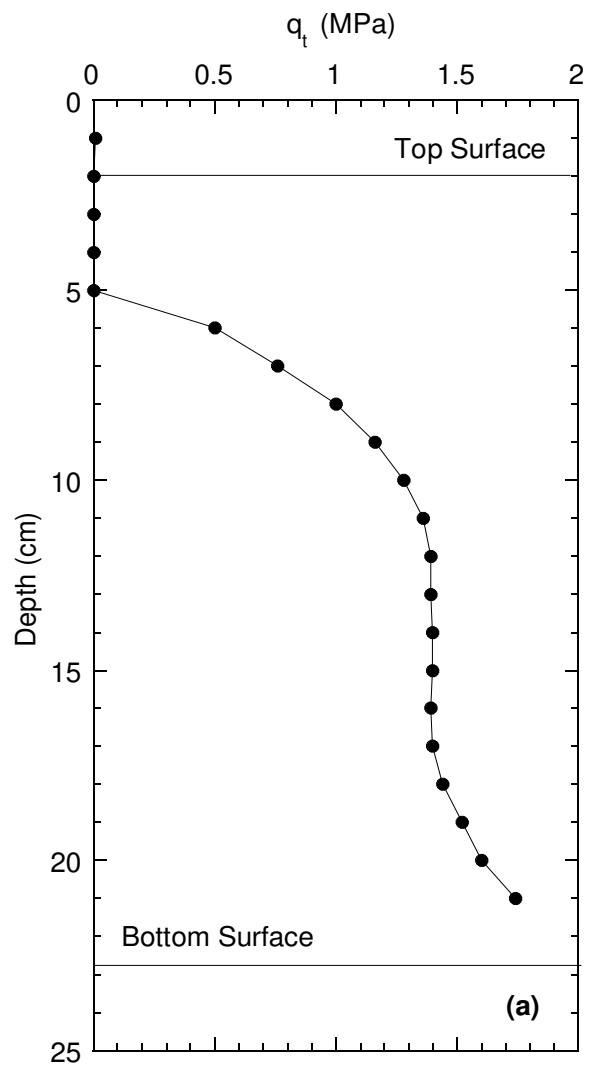


Fig. 5.12. Relationships of (a) tip resistance (q_c), (b) sleeve friction (f_s), and (c) pore water pressure as a function of penetration depth for the miniature cone penetration test on CCP consolidated under a vertical effective stress (σ'_v) of 40 kPa.



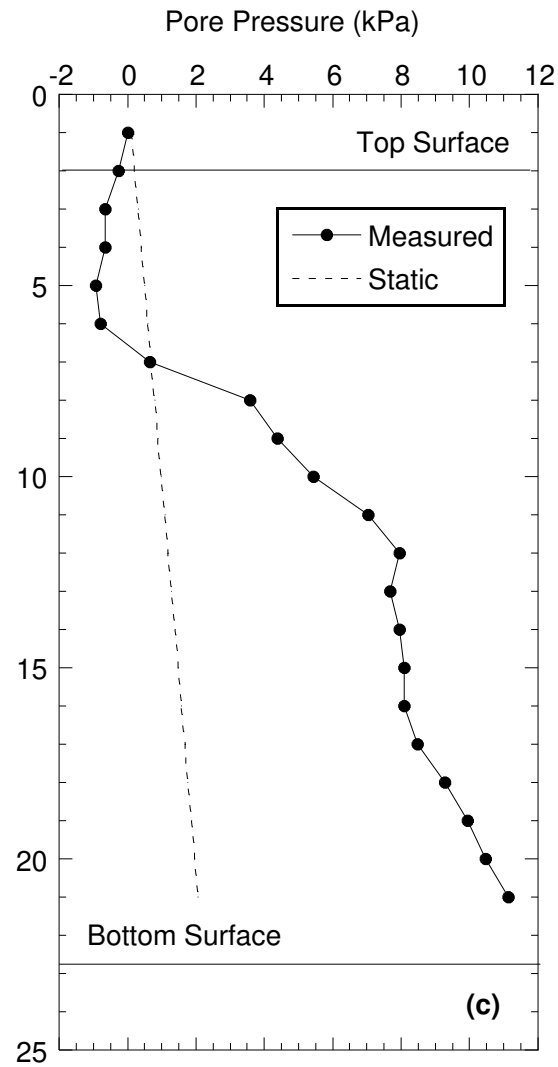


Fig. 5.13. Relationships of (a) tip resistance (q_c), (b) sleeve friction (f_s), and (c) pore water pressure as a function of penetration depth for the miniature cone penetration test on CCP consolidated under a vertical effective stress (σ'_v) of 88 kPa.

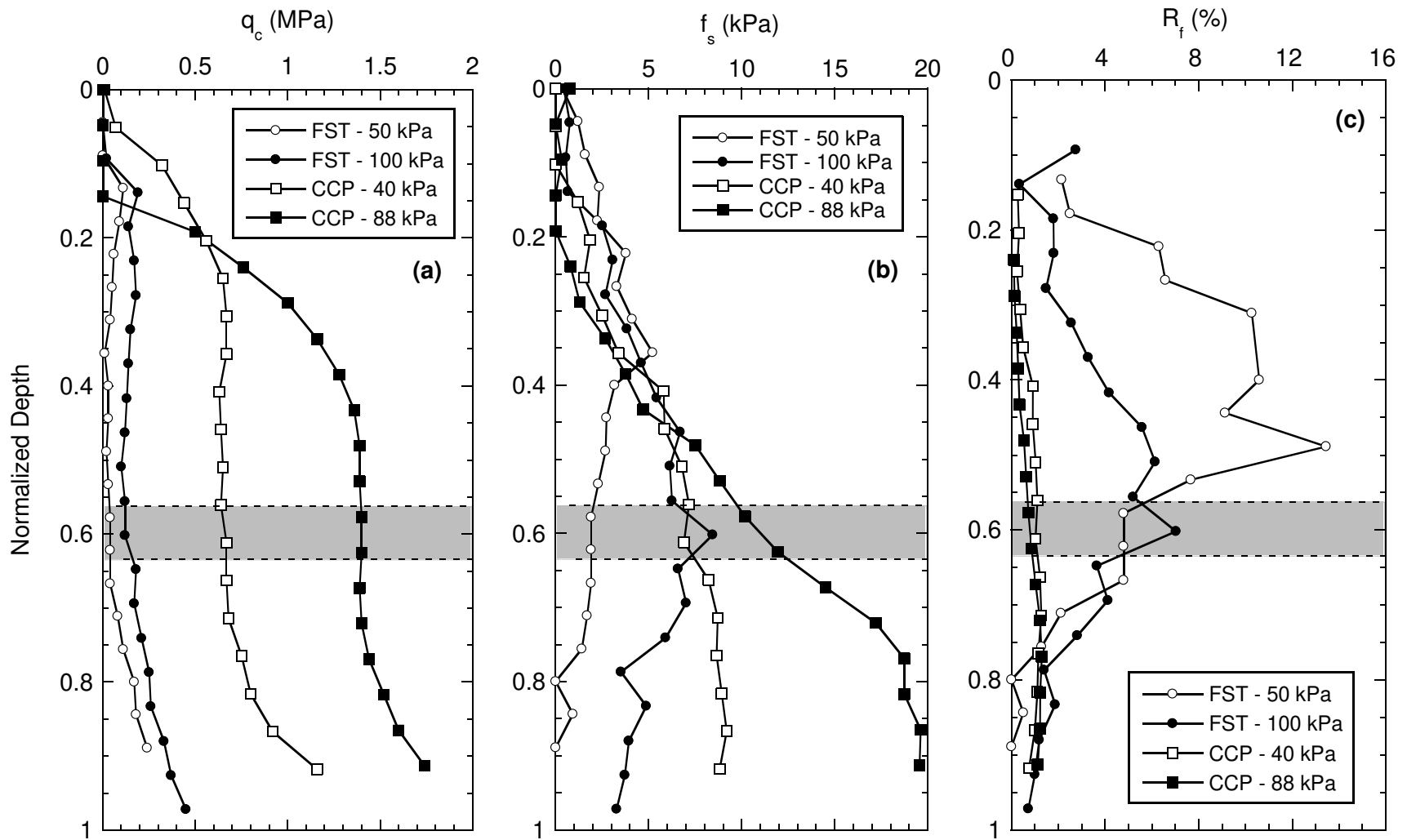


Fig. 5.14. Relationships of (a) tip resistance (q_c), (b) sleeve friction (f_s), and (c) friction ratio (R_f) as a function of normalized specimen depth for all miniature cone penetration tests on FST and CCP. Normalized specimen depth = penetration depth below specimen surface / specimen thickness. Gray area indicates the range of normalized depths at which 100% sleeve frictional resistance was mobilized.

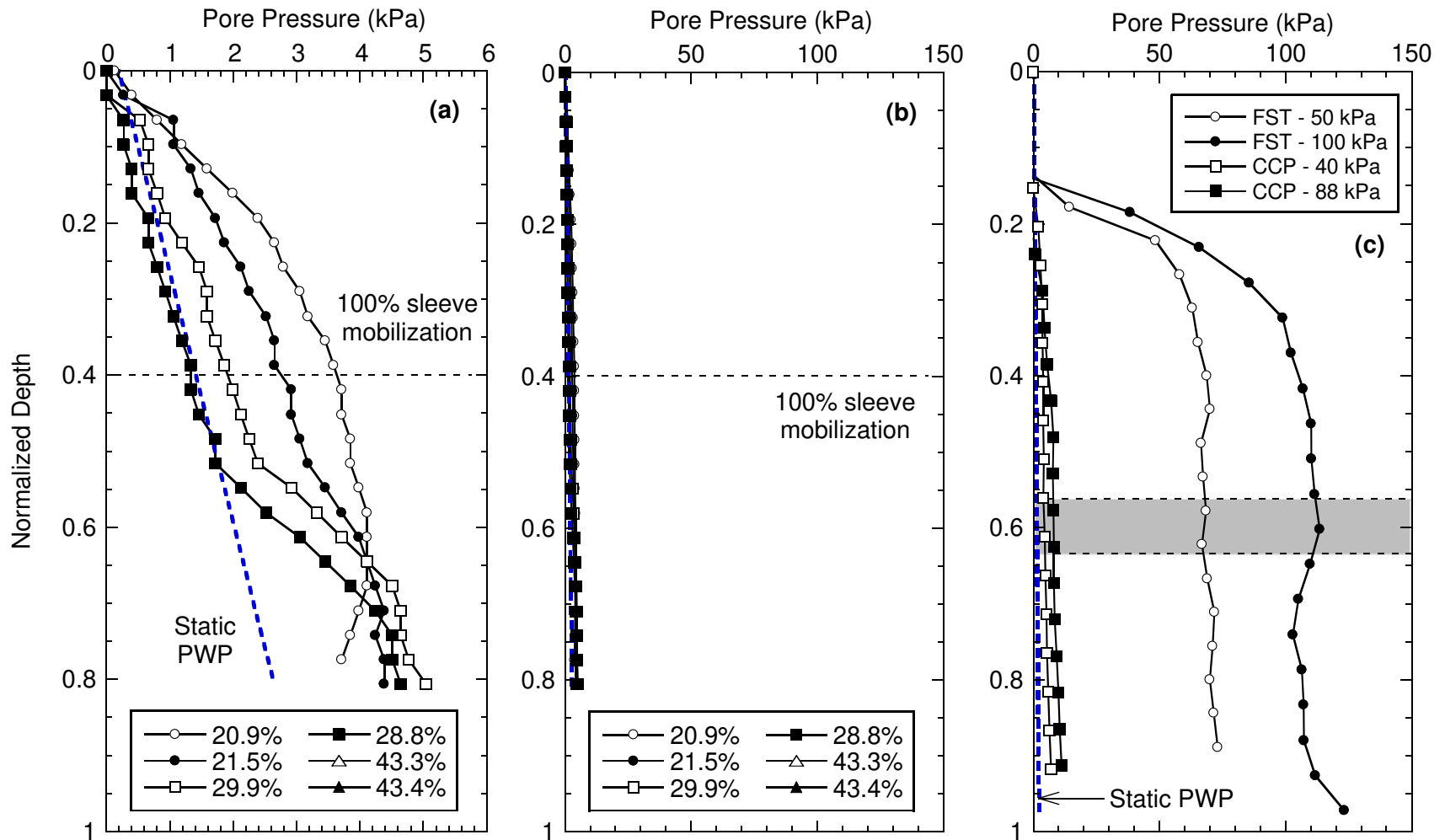


Fig. 5.15. Relationships of pore water as a function of normalized specimen depth for miniature cone penetration tests on (a) Ottawa sand, (b) Ottawa sand with a modified pore pressure scale, and (c) FST and CCP. Normalized specimen depth = penetration depth below specimen surface / specimen thickness. The modified pore pressure scale for (b) is the same scale as used in (c) to show a more direct comparison between pore pressure measured in the three different materials.

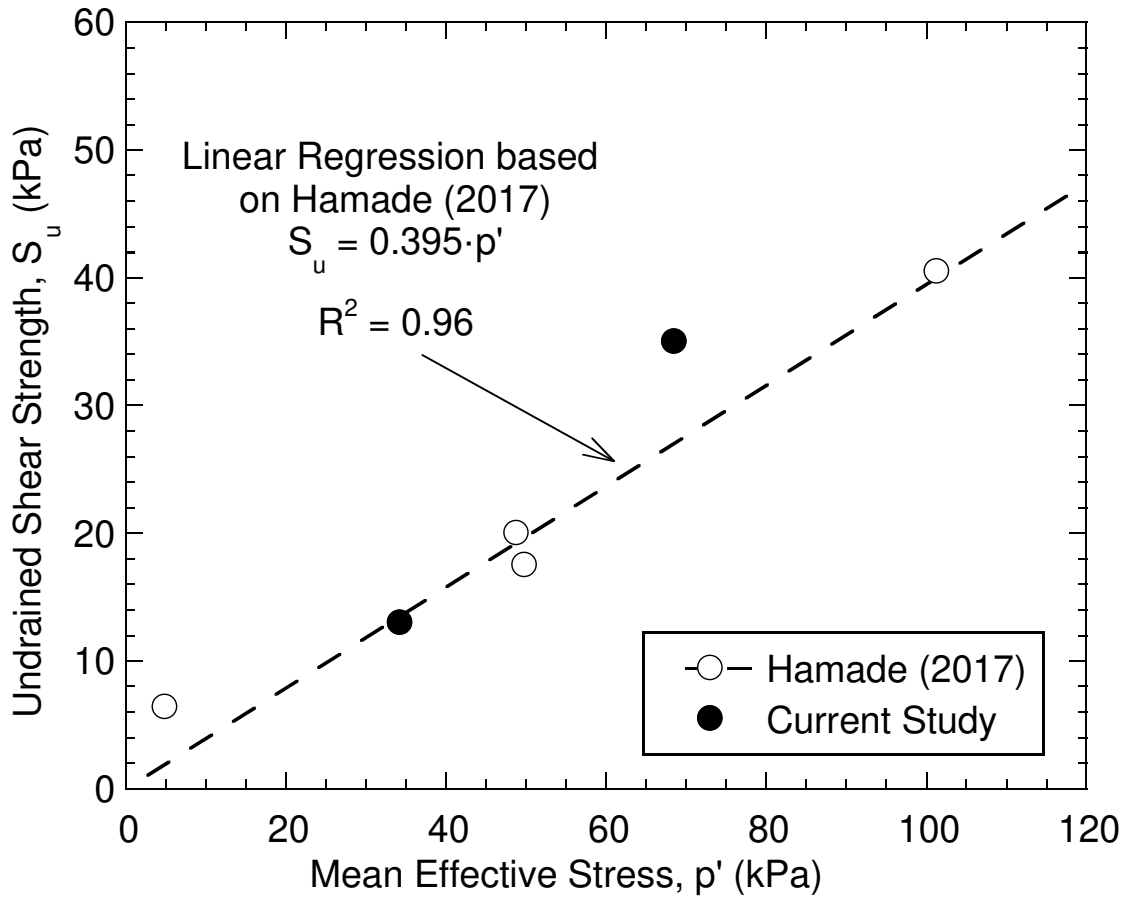


Fig. 5.16. Relationships between undrained shear strength and mean effective stress at the end of consolidation for FST based on miniature cone penetration tests in this study and consolidated undrained triaxial compression tests in Hamade (2017).

CHAPTER 6: SUMMARY, CONCLUSIONS, AND FUTURE WORK

6.1 Summary and Conclusions

The objective of this study was to design and evaluate a miniature cone penetration test (MCPT) system for evaluating fine-grained soils. The repeatability and validity of the MCPT system was assessed via tests on loosely deposited Ottawa sand. The MCPT system was further assessed via tests conducted on two fine-grained materials: fine synthetic tailings (FST) and coal combustion product (CCP). Results from the MCPTs on FST and CCP were compared to previously measured shear strength to evaluate applicability of the system for testing fine-grained materials. The following observations and conclusions were drawn from this study.

- Repeatability of the MCPT was supported via replicate tests on Ottawa sand prepared to three different relative densities. Each set of MCPTs at a given relative density yielded similar trends of tip resistance, sleeve friction, and friction ratio as a function of depth.
- Data from MCPTs on Ottawa sand were used to identify a range of specimen penetration that yielded representative tip resistance and sleeve friction. This range coincided with fully mobilized frictional resistance along the friction sleeve and no effect from the bottom specimen boundary. Tip resistance and sleeve friction compared favorably to a separate MCPT study on Ottawa sand, laboratory and field databases on cone penetration of sands, generalized soil composition and behavior, and effective stress friction angles (ϕ'). These comparisons validated the cone penetration parameters obtained from the MCPT system (tip resistance and sleeve friction).
- Pore water pressure measured during the MCPTs on Ottawa sand and CCP exhibited near hydrostatic pressure. In contrast, positive pore pressures in FST were considerably higher than hydrostatic pressure, and one to two orders of magnitude higher than the Ottawa sand and CCP. The low pore pressure in Ottawa sand and CCP were indications

of drained shear conditions during cone penetration, whereas the high positive pore pressure in FST were indications of undrained shear conditions during cone penetration.

- Undrained shear strength (S_u) estimated for FST consolidated to vertical effective stress of 50 kPa and 100 kPa were 13 kPa and 35 kPa, respectively. These S_u showed good agreement to S_u from consolidated undrained triaxial compression tests (Hamade 2017). The overall trends between S_u and mean effective stress at the end of consolidation were similar between the MCPT and triaxial tests.
- Data from the MCPTs on CCP were used to estimate $\phi' = 28.7^\circ$ and 30.4° for specimens consolidated to 40 kPa and 88 kPa, respectively. These estimated ϕ' agreed with lower-bound ϕ' measured on CCP in consolidated undrained triaxial compression (Herweynen 2018) and underestimated the average $\phi' = 36^\circ$ for a comparable range of effective stress. Thus, ϕ' for CCP via the MCPT were taken as conservative estimates.

6.2 Future Work

The following recommendations for future research are based on observations made while performing the work required for this thesis.

- The range of friction angles estimated from the MCPT for Ottawa sands were slightly high relative to the lower-end of ranges in literature for looser sands. Thus, a future step in this work should be to measure the friction angle at the same relative densities used in the MCPT to further assess prediction accuracy.
- Additional mini-piezcone penetration tests need to be conducted for CCP and FST specimens to enhance the understanding of shear behavior and increase the database.
- In order to understand scale effects potentially present in the MCPT system, the calibration chamber cell diameter should be varied and MCPTs should be conducted under similar conditions to evaluate the effect on MCPT measurements and estimated shear strength.

REFERENCES

- ASTM C778. (2017). *Standard Specification for Standard Sand*. West Conshohocken, PA: ASTM International. Retrieved from <https://www.astm.org/>
- ASTM D2487. (2017). *Standard Practice for Classification of Soils for Engineering Purposes (Unified Soil Classification System)*. West Conshohocken, PA: ASTM International. Retrieved from <https://www.astm.org/>
- ASTM D3441. (2016). *Standard Test Method for Mechanical Cone Penetration Testing of Soil*. West Conshohocken, PA: ASTM International. Retrieved from www.astm.org
- ASTM D4253. (2016). *Standard Test Methods for Maximum Index Density and Unit Weight of Soils Using a Vibratory Table*. West Conshohocken, PA: ASTM International. Retrieved from <https://www.astm.org/>
- ASTM D4254. (2016). *Standard Test Methods for Minimum Index Density and Unit Weight of Soils and Calculation of Relative Density*. West Conshohocken, PA: ASTM International. Retrieved from <https://www.astm.org/>
- ASTM D4318. (2017). *Standard Test Methods for Liquid Limit, Plastic Limit, and Plasticity Index of Soils*. West Conshohocken, PA: ASTM International. Retrieved from <https://www.astm.org/>
- ASTM D5778. (2012). *Standard Test Method for Electronic Friction Cone and Piezocone Penetration Testing of Soils*. West Conshohocken, PA: ASTM International. Retrieved from <https://www.astm.org/>
- ASTM D854. (2014). *Standard Test Methods for Specific Gravity of Soil Solids by Water Pycnometer*. West Conshohocken, PA: ASTM International. Retrieved from <https://www.astm.org/>
- Been, K., Crooks, J., Becker, D. E., & Jefferies, M. G. (1986). The cone penetration test in sands: part I, state parameter interpretation. *Geotechnique*, 36(2), 239-249.
- BS 1377. (1990). *Methods of Testing of Soils for Civil Engineering Purposes*. Milton Keneyes, UK: British Standards Institutions.
- Chapman, G. A. (1974). A Calibration Chamber for Field Testing Equipment. *Proceedings, European Symposium on Penetration Testing* (pp. 59-65). Stockholm, Sweden: National Swedish Building Research.
- Damavandi-Monfared, S. (2014). *Miniature Cone Penetration Test on Loose Sand*. London, Ontario, Canada: University of Western Ontario.
- Damavandi-Monfared, S., & Sadrekarimi, A. (2015). Development of a Miniature Cone Penetrometer for Calibration Chamber Testing. *Geotechnical Testing Journal*, 38(6), 878-892. doi:10.1520/GTJ20150036
- De Lima, D. C., & Tumay, M. T. (1991). Scale effects in cone penetration tests. *Geotechnical Engineering Congress* (pp. 38-51). Boulder, CO: ASCE.

- EPRI. (2012). *Geotechnical Properties of Fly Ash and Potential for Static Liuefaction: Volume 1- Summary and Conclusions*. Palo Alto, CA: EPRI.
- Ghionna, V. N., & Jamiolkowski, M. (1991). A critical appraisal of calibration chamber testing of sands. *Proceedings of the First International Symposium on Calibration Chamber Testing/ISOCCCT1* (pp. 13-40). Potsdam, New York: An-Bin Huang Ed.
- Gorman, C. T., Drnevich, V. P., & Hopkins, T. C. (1975). Measurement of in-situ shear strength. *In-situ Measurement of Soil Properties* (pp. 139-140). Reston, Virginia: ASCE.
- H. Gorakhki, M., & Bareither, C. A. (2018). Compression Behavior of Mine Tailings Amended with Cementitious Binders. *Geotechnical and Geological Engineering*, 27-47.
- Hamade, M. (2017). *Undrained Shear Behavior of Mixed Mine Waste Rock and Tailings*. Fort Collins, Colorado: Master of Science Thesis, Colorado State University.
- Herweynen, W. J. (2018). *Shear Strength of Coal Combustion Product By Vane Shear*. Fort Collins, Colorado: Master of Science Thesis, Colorado State University.
- Holden, J. C. (1971). *Laboratory Research on Static Cone Penetrometers*. University of Florida, Gainesville, Florida, USA: Department of Civil Engineering, Internal Report CE-SM-71-1.
- Huang, A. B. (1986). *Laboratory pressuremeter experiments in clay soils*. West Lafayette, Indiana: Ph.D. Dissertationn, Purdue University.
- Jamiolkowski, M., Lopresti, D., & Manassero, M. (2001). Evaluation of relative density and shear strength of sands from cone penetration test and flat dilatometer test. *Soil Behavior and Soft Ground Construction (GSP 119)* (pp. 201-238). Reston, VA: ASCE.
- Kim, K., Prezzi, M., Salgado, R., & Lee, W. (2008). Effect of penetration rate on cone resistance in saturated clayey soils. *Journal of Geotechnical and Geoenvironmental Engineering*, 134(8), 1142-1153.
- Kulhawy, F. H., & Mayne, P. W. (1990). *Manual on Estimating Soil Properties for Foundation Design*. Palo Alto: Report EPRI EL-6800, Electric Power Research Institute.
- Kumar, J., & Raju, K. (2009). Miniature cone tip resistance of sand with fly ash using triaxial setup. *Can. Geotech. J.*, 46, 231-240.
- Lambrechts, J. R., & Leonards, G. A. (1978). Effects of stress history on deformation of sand. *Journal Geotechnical Engineering*, 104(11), 1371-1387.
- Lunne, T., Robertson, P. K., & Powell, J. M. (1997). *The Cone Penetration Test in Geotechnical Practice*. New York: EF Spon/Blackie Academic, Routledge Publishing.
- Mayne, P. W. (2006). The 2006 James K. Mitchell Lecture: Undisturbed Sand Strength from Seismic Cone Tests. *GeoShanghai International Conference* (pp. 1-36). Shanghai, China: ASCE.
- Mayne, P. W. (2005). Integrated ground behavior: in-situ and lab tests. *Deformation Characteristics of Geomaterials*, 155-177.
- Mayne, P. W. (2007). *Cone penetration testing - a synthesis of highway practice*. Washington, DC: NCHRP Synthesis 368, Transportation Research Board.

- Mayne, P. W. (2014). Interpretation of geotechnical parameters from seismic piezocone tests. *Proceedings, 3rd International Symposium on Cone Penetration Testing* (pp. 47-73). Las Vegas: ISSMGE Technical Committee TC 102, Edited by P.K. Robertson and K.I. Cabal.
- McManus, K. J., & Kulhawy, F. H. (1991). A Cohesive Soil for Large-Size Laboratory Deposits. *Geotechnical Testing Journal, GTJODJ*, 15(1), 26-34.
- Meigh, A. C. (1987). *Cone penetration testing-methods and interpretation*. Buttersworths, London: Construction Industries Research and Information Association.
- Randolph, M. F., & Hope, S. (2004). Effect of cone velocity on cone resistance and excess pore pressures. *Proc., Int. Symp. on Eng. Practice and Performance of Soft Deposits*, (pp. 147-152). Yodogawa Kogisha, Osaka.
- Robertson, P. K. (1990). Soil classification using the cone penetration test. *Canadian Geotechnical Journal*, 27(1), 151-158.
- Robertson, P. K., & Cabal, K. L. (2015). *Guide to Cone Penetration Testing for Geotechnical Engineering*. Signal Hill, California : Gregg Drilling & Testing, Inc.
- Salgado, R., Bandini, P., & Karim, A. (2000). Shear strength and stiffness of silty sand. *Journal of Geotechnical and Geoenvironmental Engineering*, 451-462.
- Salgado, R., Mitchell, J. K., & Jamiolkowski, M. (1998). Calibration chamber size effects on penetration resistance in sand. *Journal of Geotechnical and Geoenvironmental Engineering*, 124(9), 878-888.
- Scherif, M. A., Ishibashi, I., & Ryden , D. E. (1974). *Coefficient of lateral earth pressure at rest in cohesionless soils*. Seattle, WA : Soil Engineering Research Report No. 10; University of Washington.
- Schmertmann, J. H. (1978). *Study of feasibility of using wissa-type piezometer probe to identify liquefaction potential of saturated fine sands*. Vicksburg, Miss: U.S. Army Engr. Wtwys. Experiment Station.
- Senneset, K., & Janbu, N. (1985). Shear strength parameters obtained from static cone penetration tests. *Strength testing of marine sediments; Laboratory and in-situ measurements* (pp. 41-54). San Diego: ASTM STP 833.
- Senneset, K., Sandaven, R., & Janbu, N. (1989). *Evaluation of soil parameters from piezocone tests*. Washington DC: Transportation Research Record 1235.
- Tian, Z. (2017). *Seepage-induced consolidation test mine tailings*. Fort Collins, Colorado: Master of Science Thesis, Colorado State University.
- Tufenkjian, M. R., & Thampson, D. J. (2005). Shallow penetration resistance of a minicone in sand. *Proceedings of the 16th International Conference on Soil Mechanics and Geotechnical Engineering*, (p. 89). Osaka, Japan.
- Tumay, M. T., & de Lima, D. C. (1992). *Calibration and Implementation of Miniature Electric Cone Penetrometer and Development, Fabrication and Verification of the LSU In-situ Testing Calibration Chamber (LSU/ CALCHAS)*. 240: LTRC/FHWA Report No. GE-92/08.

- Tumay, M. T., Kurup, P. U., & Boggess, R. L. (1998). A continuous intrusion electronic miniature CPT. *Geotechnical Site Characterization, 2*, pp. 1183-1188. Balkema, Rotterdam, The Netherlands.
- Uzielli, M., Mayne, P. W., & Cassidy, M. J. (2013). Probabilistic assessment of design strengths for sands from in-situ testing data. In *Modern Geotechnical Codes of Practice – Development and Calibration* (pp. 214-227). Amsterdam: Taylor & Francis.
- Veismanis, A. (1974). Laboratory investigation of electrical friction-cone penetrometers in sands. *1st European Symposium on Penetration Testing* (pp. 407-419). European Society of Soil Mechanics and Foundation Engineering.
- Vlasblom, A. (1985). *The Electrical Penetrometer: A Historical Account of Its Development*. The Netherlands: Delft Soil Mechanics Laboratory.

APPENDIX A: DESIGN DRAWINGS

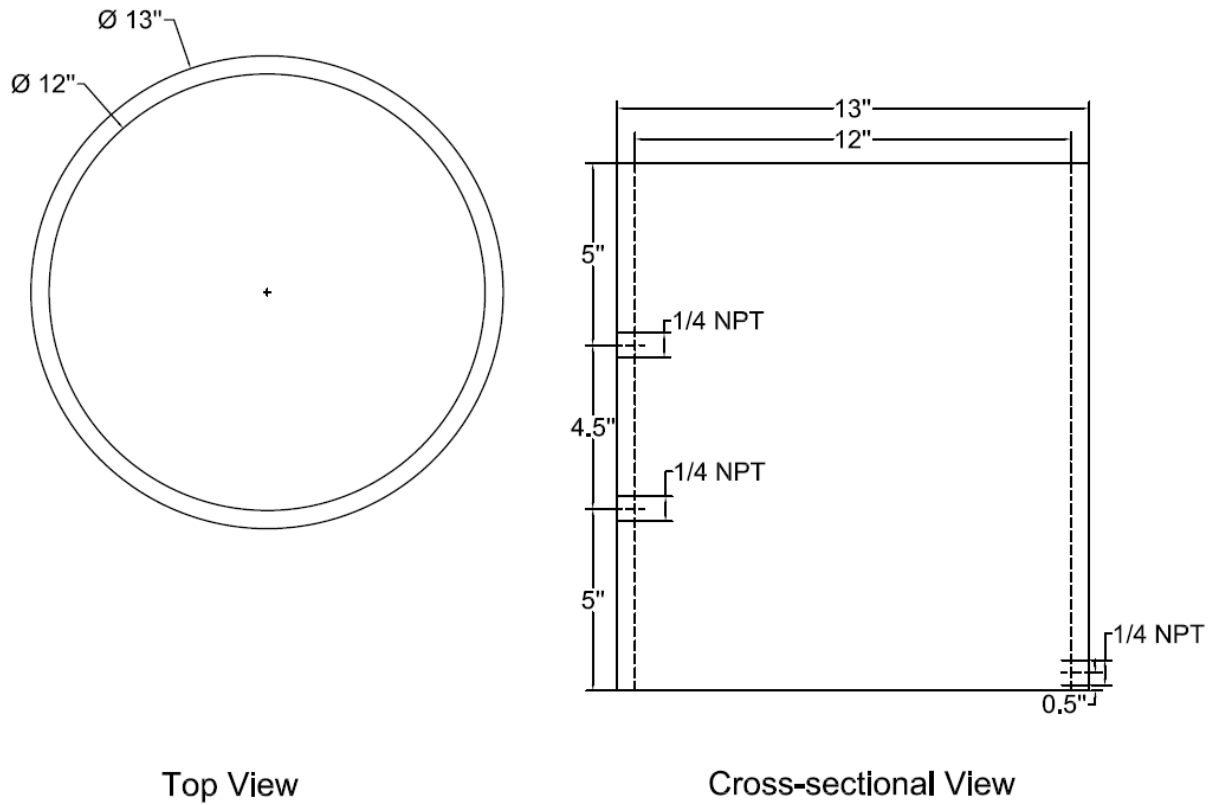
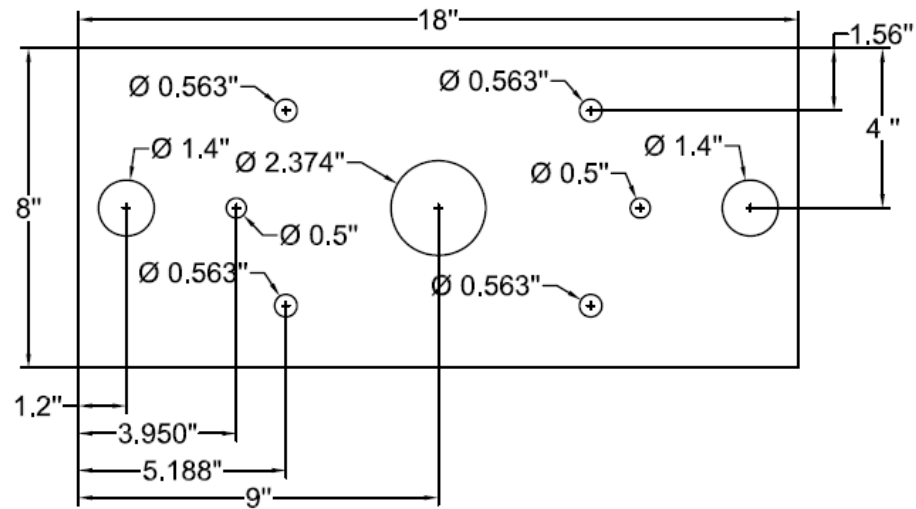
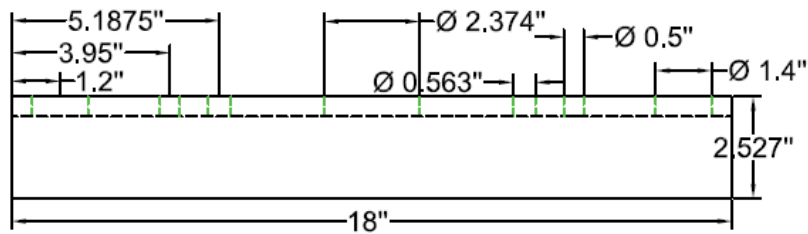


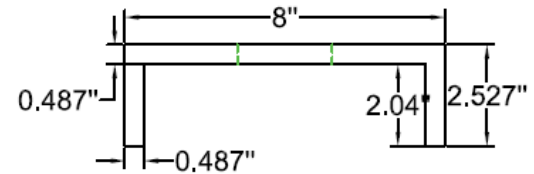
Fig. A.1. Dimensions of the specimen cell.



Top View

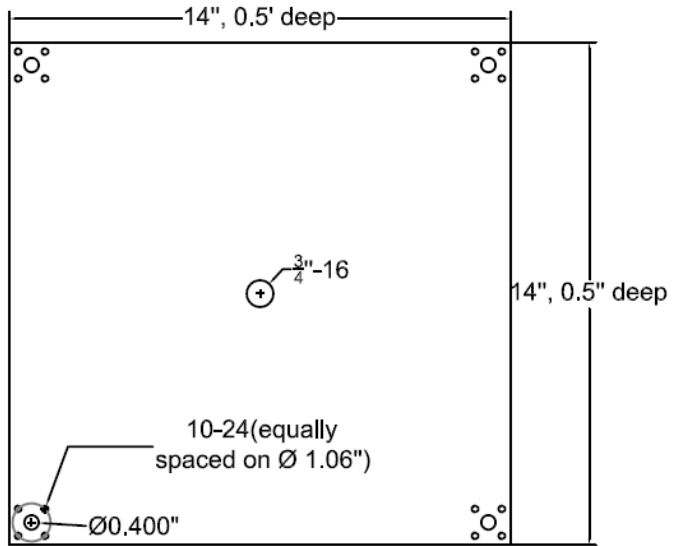


Cross-sectional View

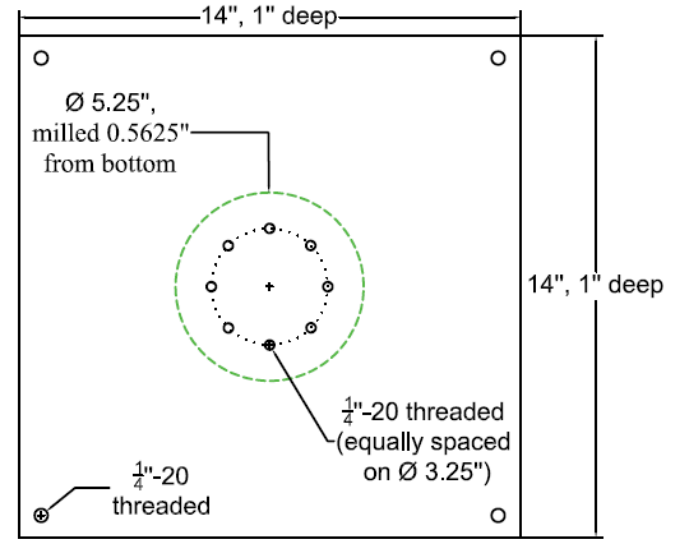


Front View

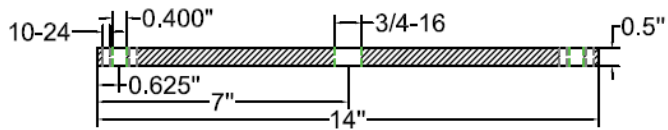
Fig. A.2. Drawing views of the cross bar from different perspectives.



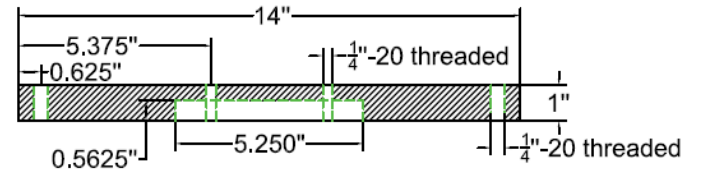
Top View



Top View



Cross-sectional View



Cross-sectional View

Fig. A.3. Drawing views of the bottom plates from different perspectives

APPENDIX B: CONSOLIDATION DATA

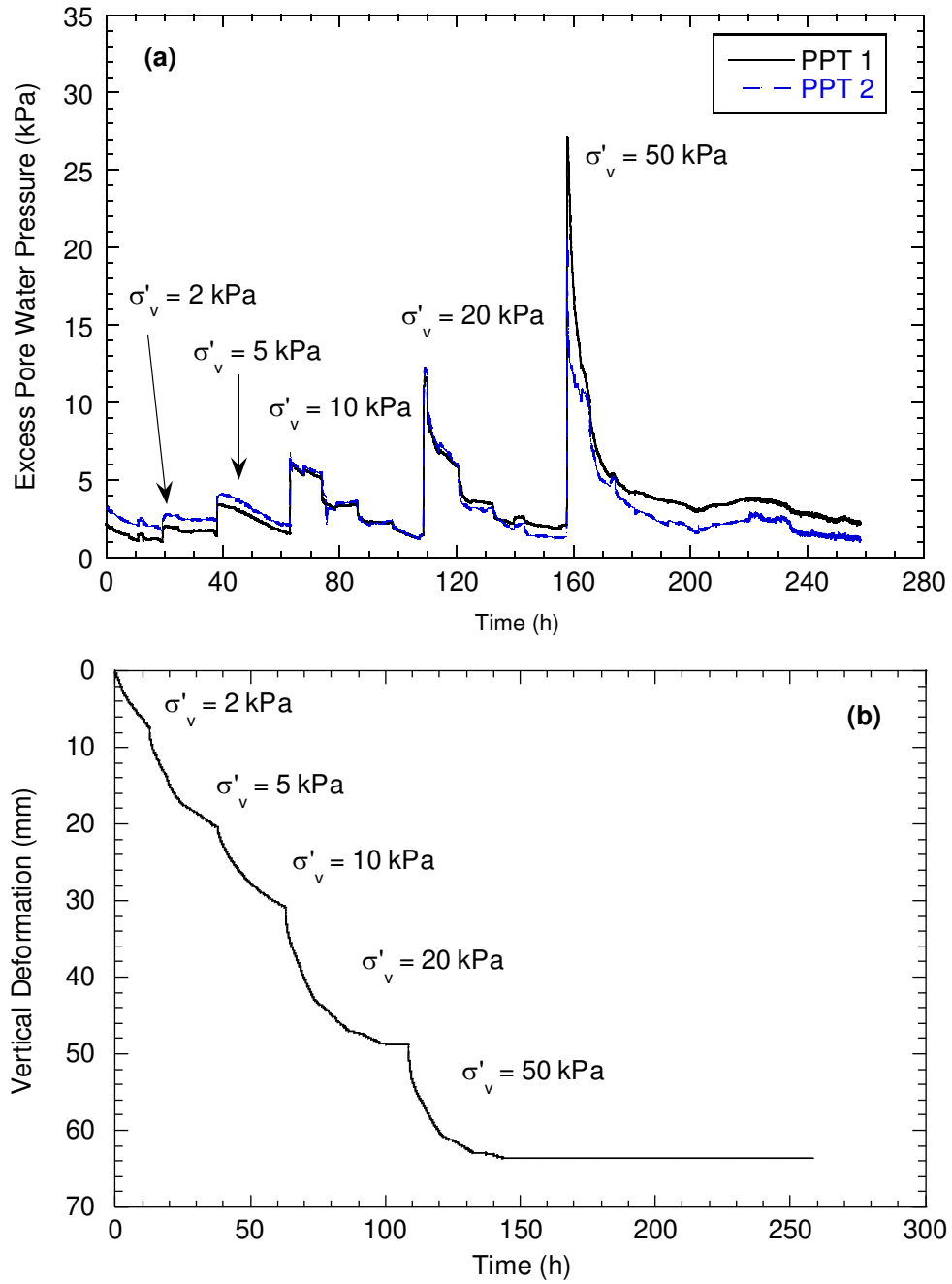


Fig. B.1. Temporal trends of (a) excess pore water pressure and (b) vertical deformation of the specimen surface for the FST in the miniature cone penetration test tested under a vertical effective stress (σ'_v) of 50 kPa.

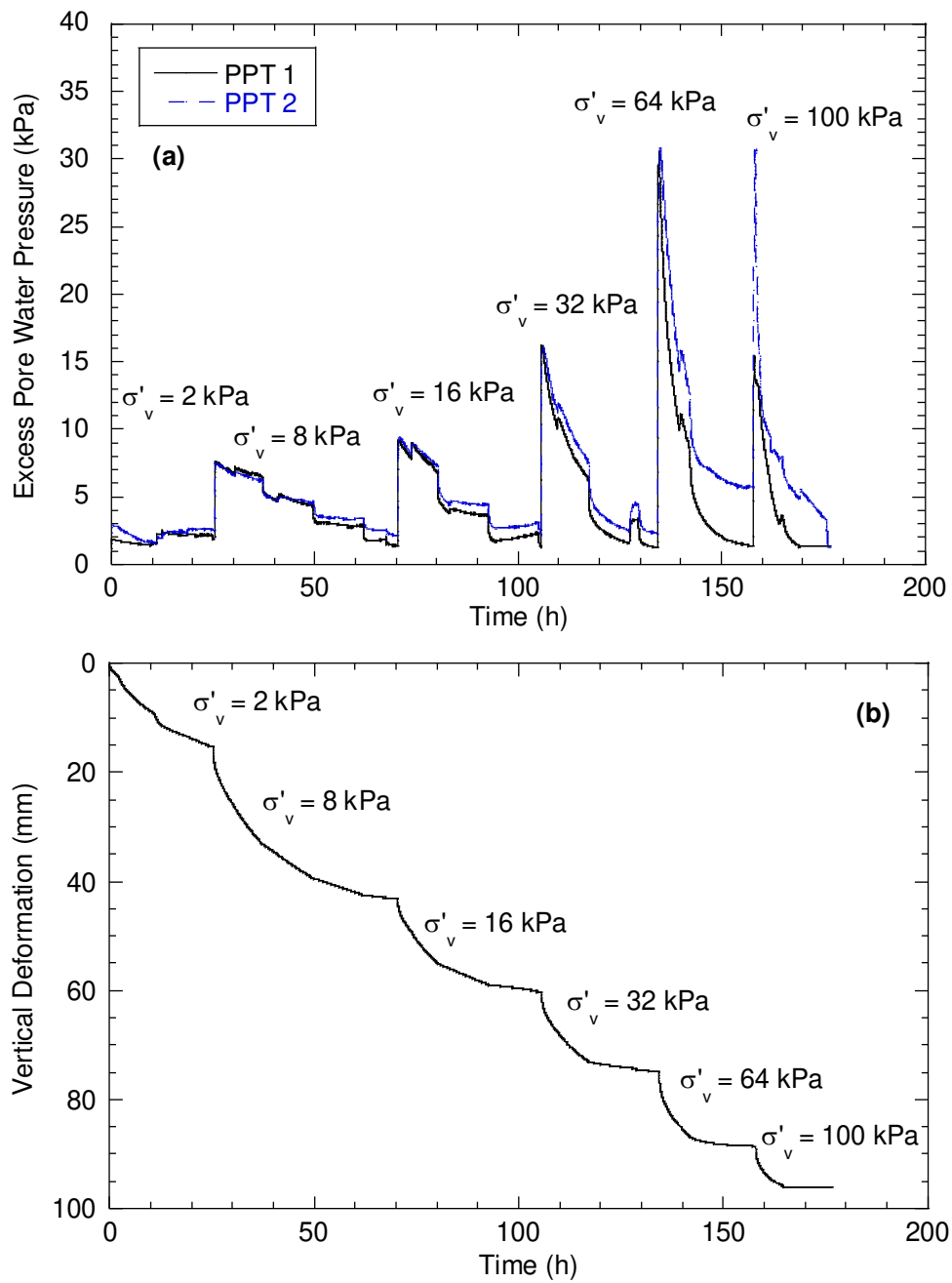


Fig. B.2. Temporal trends of (a) excess pore water pressure and (b) vertical deformation of the specimen surface for the FST in the miniature cone penetration test tested under a vertical effective stress (σ'_v) of 100 kPa.

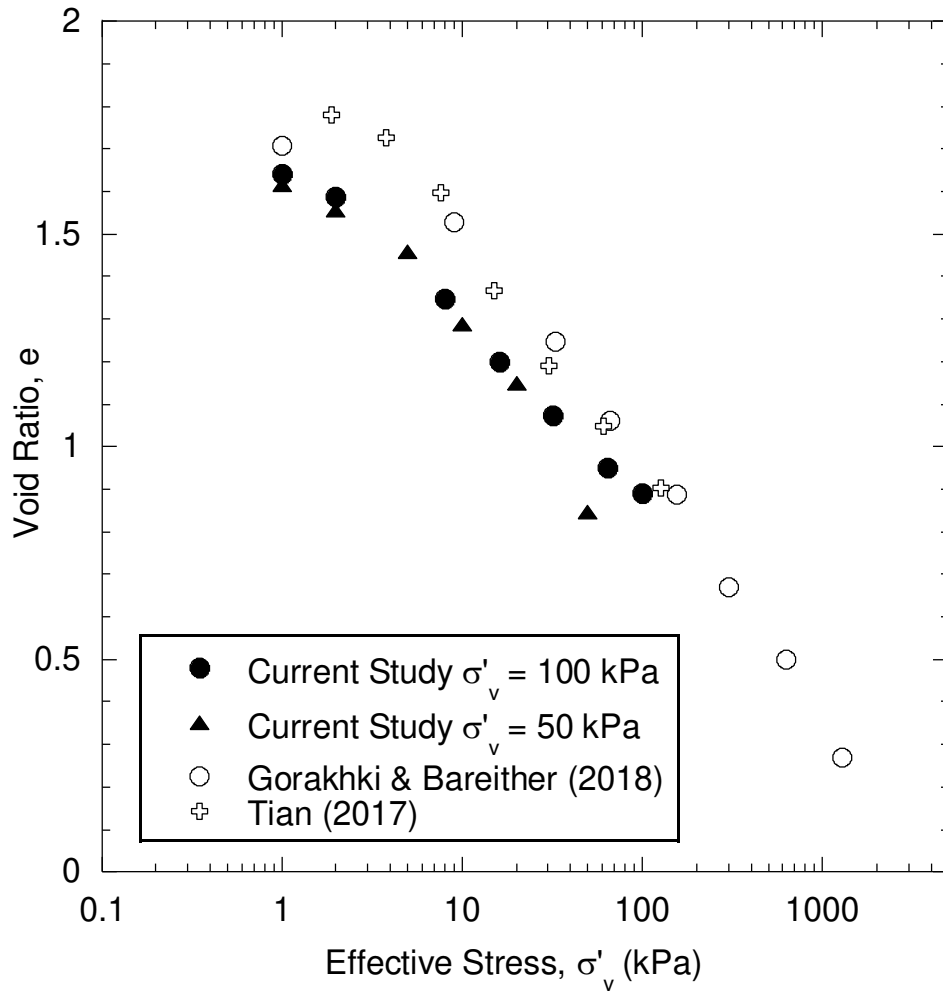


Fig. B.3. Comparison of void ratio versus vertical effective stress data for FST from the two miniature cone penetration tests and odometer data from Gorakhki and Bareither (2018) and Tian (2017).

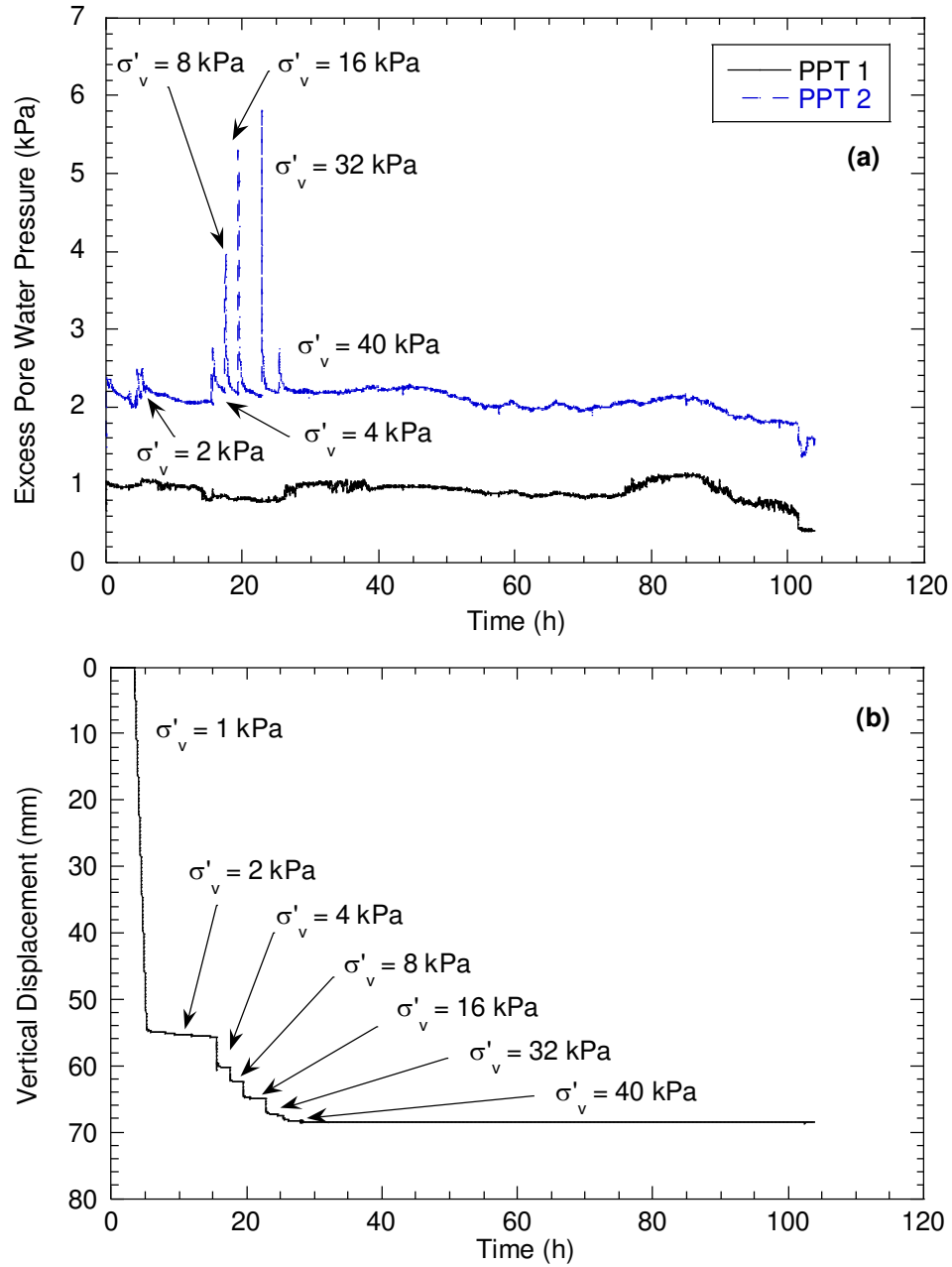


Fig. B.4. Temporal trends of (a) excess pore water pressure and (b) vertical deformation of the specimen surface for the CCP in the miniature cone penetration test tested under a vertical effective stress (σ'_v) of 40 kPa.

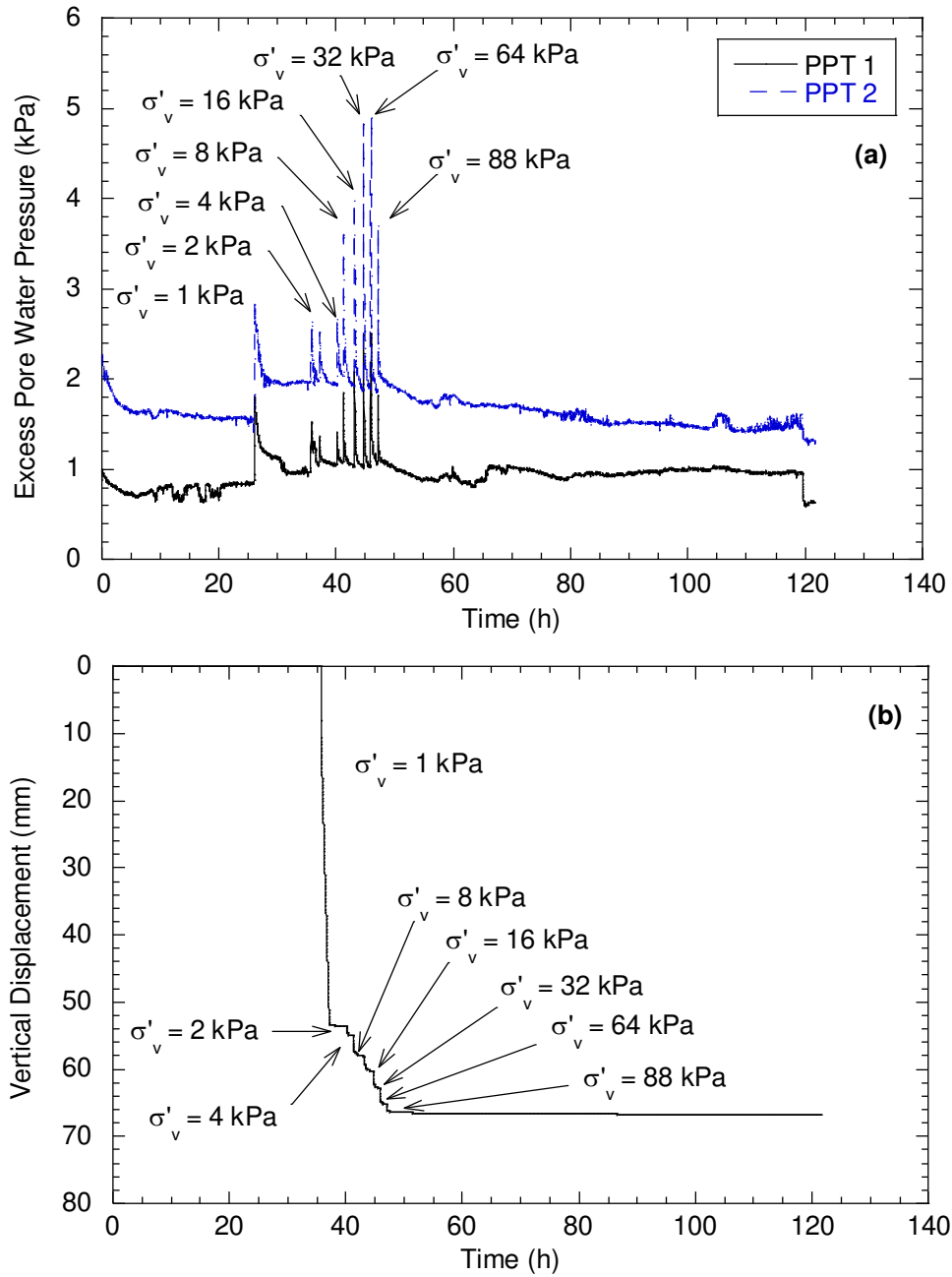


Fig. B.5. Temporal trends of (a) excess pore water pressure and (b) vertical deformation of the specimen surface for the CCP in the miniature cone penetration test tested under a vertical effective stress (σ'_v) of 88 kPa.

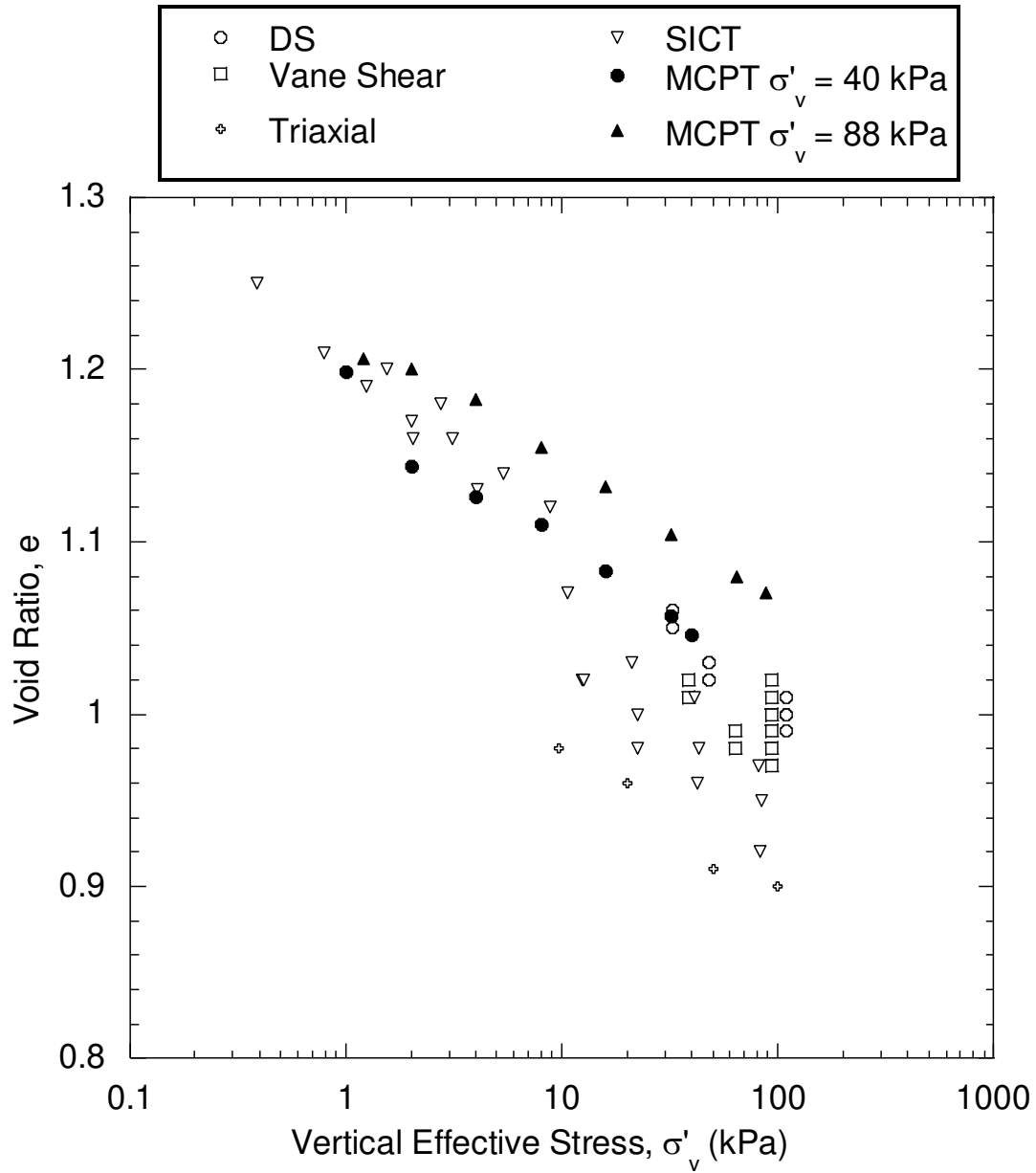


Fig. B.6. Comparison of void ratio versus vertical effective stress data for CCP from miniature cone penetration tests and seepage-induced consolidation (SICT), direct shear (DS), triaxial, and vane shear tests conducted by Herweynen (2018).